CRANFIELD UNIVERSITY

MONICA MONDRAGO QUEVEDO

PROBABILISTIC MODELLING OF GEOTECHNICAL CONDITIONS FOR OFFSHORE WIND TURBINE SUPPORT STRUCTURES

SCHOOL OF ENGINEERING

MSc by Research

MSc THESIS

Academic Year: 2013 - 2014

Supervisor: Dr Athanasios Kolios

May 2014

CRANFIELD UNIVERSITY

SCHOOL OF ENGINEERING
MSc by Research

MSc Thesis

Academic Year 2013 - 2014

MONICA MONDRAGO QUEVEDO

PROBABILISTIC MODELLING OF GEOTECHNICAL CONDITIONS FOR OFFSHORE WIND TURBINE SUPPORT STRUCTURES

Supervisor: Dr Athanasios Kolios
May 2014

ABSTRACT

The geotechnical conditions of the soil can fluctuate greatly across the wind farm. This is an issue since geotechnical modelling is the base of the structural design of an offshore wind farm, and the efficient installation of the wind turbines depends on its accuracy. This paper deals with the characterization of the seabed, predicting the soil properties over the total affected area by a wind farm, with the challenge to reduce the required data samples in the site investigation under the number of installed wind turbines, to reduce its cost.

It is compared the prediction outcome from two different interpolation methods, kriging and radial basis function, assessing their accuracy by the Mean-Squared Error and the Goodness-of-Prediction Estimate, as well as with a visual examination of their mapping; obtaining higher accuracy for radial basis function and reducing to half the required sample points, from the initial value of installed wind turbines.

In a second stage it is studied the soil effect over the foundation, analyzing the results from a FEA, where different geometries of the structure are compared submitted to different load cases to check its limit states. Those results show that the foundation cost can increase four times due to the soil conditions, taking into account only the steel volume, and demonstrating how important is the soil characterization in the foundation design, as it gives the chance to relocate those wind turbines that require more expensive foundations.

Keywords:

Kriging, RBF, seabed characterization, wind turbines foundation design

ACKNOWLEDGEMENTS

“If one does not know to which port one is sailing, no wind is favourable”
Lucius Annæus Seneca

I want to express my deepest gratitude to those winds which have sailed with me and leaded me to this port.

Firstly, I want to deeply thank Dr Athanasios Kolios, my supervisor, who has been the main wind on this trip. His help, guidance and encouragement have been the key that has allowed me to complete this project. Since the beginning he put all his trust on me and defended my capacity and abilities to work. His ability to motivate me has been unique, even in the worst moments. The words “thank you” are not enough to express my gratitude to him.

I want also to express my deepest gratitude to my parents, winds that have guided me in my life trip. Without them would have been impossible even to begin this project. Especially I want to dedicate this work to my father, who had the dream to see that I am engineer. He met his dream, and although his wind stopped blowing in the middle of this trip, I hope his guidance helps me to meet mines.

I could never forget my sister, my twin, my friend, the small gust that never stops blowing and always keeps me sailing.

You can feel it on your face, against your body or playing with your hair. The power of the wind can send a kite into the sky, bring a sailboat to the port or supply electricity to our homes.

Monica

TABLE OF CONTENTS

LIST OF FIGURES

LIST OF TABLES

ABBREVIATIONS

3D	Three dimensions
ALARP	As Low As Reasonably Practicable
ALS	Accidental Limit State
API	American Petroleum Institute
BGS	British Geological Survey
BSH	Bundesamt Für Seeschifffahrt Und Hydrographie
DECC	Department of Energy & Climate Change
DNV	Det Norske Veritas
EC	European Commission
ECS	Committee for Standardisation
EU	European Union
EWEA	European Wind Energy Association
FLS	Fatigue Limit State
G	Goodness-of-Prediction Estimate
GI	Geographic Information
LCOE	Levelised Cost of Electricity
MAREMAP	Marine Environmental Mapping Programme
MSE	Mean-Squared Error
NERC	Natural Environment Council
OWT	Offshore Wind Turbine
RBD	Reliability-Based Desig
RBF	Radial Basis Function
RP	Recommended Practice
SLS	Serviceability Limit State
TP	Transition Piece
UK	United Kingdom
ULS	Ultimate Limit State

1 INTRODUCTION

As European Directive 2009/28/EC established in 2009, all member countries from European Union will have to ensure that 20% of total consumed energy is satisfied from renewable energy sources, by 2020, under the requirement of better cost effective (Department of Energy & Climate Change, 2011).

Thanks to the energy policy toward a higher participation of renewable energy in the overall energy production, the European Union (EU) finished 2013 with 117.3 GW of installed wind energy capacity, enough to cover 8% of the EU's electricity consumption ((EWEA), 2014).

Due to the suitable locations for large wind energy production, preservation of landscape, higher wind speed, less turbulence intensity and insignificant acoustic emissions, offshore wind energy is leaving the wind resources on land behind.

UK has been the leader in offshore wind since October 2008, with a largest capacity than the rest of the world combined. Currently, UK has 3.65GW operating across 22 wind farms. UK is on the top of offshore wind and it is planning to continue ahead, with other 5.7GW capacity under construction and 12.3GW under planning (July 2014) (RenewableUK, 2014).

On the other hand there are extra costs involved with the installation of offshore wind energy, i.e in the support structure due to the additional hydrodynamic loading, installation and maintenance due to the transportation and limited access and the need of offshore electrical transmission.

Furthermore, as (The Crown Estate, 2012) indicates, the costs of offshore wind have been increasing in UK since the first wind farm was installed, by higher capacity wind turbines and moving to deeper water locations, reaching in the latest wind farm projects £140/MWh (measured cost as LCOE (Levelised Cost of Electricity) - lifetime cost of the project per unit of energy generated). If the costs continue rising and taking into account the wider financial condition, the industry in UK will not be able to meet the stipulated targets, because each time it will be less attractive to the financial parts.

So, the current challenge becomes to bring costs down and deployment up, to achieve the goals by 2020, at the same time, producing more renewable energy gives to UK greater independence from fuel price fluctuation, which protects consumers, it will create new job opportunities and businesses in this sector, as well as it will help with the carbon reduction objectives.

While technical challenges are accomplished, the LCOE is expected to drop throughout time, with the objective to accomplish £100/MWh by 2020 (Department of Energy & Climate Change, 2011).

Offshore wind industry is a sector in its infancy and it has been operating based on the oil and gas industry standards and also with its products. This does not help to develop the sector or reduce its costs. To reduce the cost is necessary to achieve an efficient structural design. As wind farms have been working, geotechnical survey data were available just on each turbine location, which leads to uncertainties in cable layout design. One of the opportunities to reduce the costs of offshore wind falls on better knowledge of the seabed conditions, because past projects showed unexpected increased cost due to the lack of soil characterization (The Crown Estate, 2012).

According to (Randolph, Cassidy, Gourvenec, & Erbrich, 2005), the costs for the vessel for the site investigation are between $250,000 and $500,000 per day; although these figures are not up-to-date, they give a very good indication of the cost of intervention. Due to this high cost, another chance to decrease the energy cost is to reduce the spent amount of money in the site investigation.

The wind energy production depends on the geographical location, because natural resources are not everywhere. But since the wind turbines have enlarged, reaching 125 m rotor diameter, producing 5000kW by 2015 (International Energy Agency, 2013); the production of the wind farms has increased so much that it can appear overproduction, which means the wind farm is able to produce more energy than the site demand. There are two solutions in that case to not to lose energy. One it can be installing a storage system, which requires a high extra cost; and another one, geographical dispersion, which increases the cost of interconnection cabling in the wind farm

collection system (see figure 1), but it is technically beneficial (Van Assen, 2012). This implies to change the location of some wind turbines, in order to place them where the energy it can be introduced to the grid; but at the same time, it requires a wider knowledge on the soil conditions.

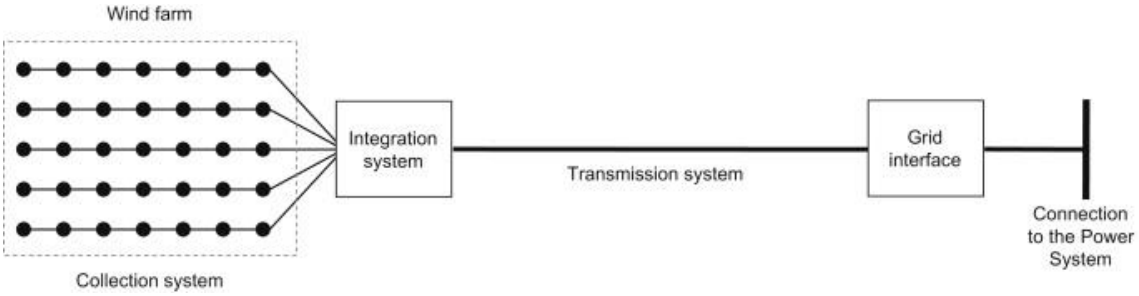

Figure 1: Offshore wind farm general layout
Source: (Dicorato, Forte, Pisani, & Trovato, 2011)

1.1 Background

Until earlier past century, most of the engineering judgements in design and construction were based on experience and precedents. Since World War II, the judgement has changed significantly as a result of theoretical, experimental and developments in engineering; although it is still indispensable in site characterisation, selection of appropriate parameters and analysis methods, without forgetting the critical evaluation of the results of observations or analysis.

The design objective is to ensure the structure performs satisfactorily within a specified period of time. The first traditional deterministic design codes were based on safety factors at the design stage, to reduce the risk of potential failure. Factors of safety can be misleading, because sometimes are recommended without reference to the loads and their evaluation, the analysis method, the method of property evaluation, and so on (Kulhawy & Phoon, 1996). The method was constructed for the engineer to go through the process of considering each factor in detail and this process itself can lead to inconsistencies.

Another doubt to trust this method lies in the relationship between the safety factor and the level of risk, because a higher safety factor can not to imply a smaller level of risk, considering that at the same time can be present larger uncertainties in the design that consume the security of the factor.

With the evolution of structural safety concepts, those traditional codes have been gradually replaced by reliability-based design (RBD) codes, which provide consistent assurance of safety based on probabilistic analysis.

Here appears the concept of limit state design which requires identifying all the limit states or potential failure modes, check separately each limit state and show that the possibility of occurrence of each limit state is limited.

Oil and gas industry has already a large developed career in offshore construction with experience in very deep water locations. On the other hand, near shore has experience on hydrodynamic loading where wave action still affects the seabed. But the offshore wind turbine (OWT) structure is placed in the intermediate water depths with different characteristics due its location, then the design, construction and installation will follow different processes (Henderson & Camp, 2001).

In general, every structure must follow the technical rules collected in the Eurocodes, which are developed by the European Committee for Standardisation (ECS) for the structural design in the EU, but these ones are based on the structural material and they do not give specific instructions for the different types of structures.

For OWT structures there is not available any mandatory code to follow in the design process, but partnerships as Det Norske Veritas (DNV) has developed some guidelines and standards, based on the experience already achieved by the industry, to guide the engineer in the design process. The general document for offshore wind energy is DNV-OS-J101, Design of Offshore Wind Turbine Structures (2013).

This standard considers four limit states:

- Ultimate limit state (ULS), which verify the structure under maximum load.
- Fatigue limit state (FLS), which correspond to the failure due to the cyclic loading.
- Accidental limit state (ALS), which study the maximum loading capacity under accidental loads.
- Serviceability limit state (SLS), which corresponds to the capacity under normal use.

Despite the growth in offshore wind industry, there are still substantial uncertainties related to the foundation design due to the offshore environment concerning hydrodynamic loading, soil characterisation and the issue of the transition piece in monopile foundations (Carswell, Arwade, DeGroot, & Lackner, 2014; Negro, Gutierrez, Esteban, & Matutano, 2014).

The transition piece is the connection element between the tower and the pile for the monopile support structures, which represents the main weakness for these foundations due to under wind and waves dynamic loads, the grout inside the piece crumbles (Negro, Gutierrez, Esteban, & Matutano, 2014). Nowadays there are not clear solutions for this, but it is being dealt with new grout or conical pieces instead of tubular.

Hydrodynamic loads in OWT mainly come from waves and currents, but other sources like ice drift can also appear. The calculation and determination of the design wave loads is a complex undertaking, where both extreme and fatigue load cases have to be considered (Henderson & Camp, 2001).

For small waves in deep waters, the Airy wave model is sufficient for calculating the kinematic by its design wave (Mader, 2005), but as wave heights and lengths increase by the water depth, other methods need to be considered. As (Henderson & Zaaijer, 2008) indicate, from the available methods to calculate the hydrodynamic loads, the widely used are Morrison's method and diffraction theory. Usually for slender structures, such as monopiles or tripods, the

appropriate method is Morrison, while for structures such as gravity base, which are massive with significant specific surface, the diffraction theory is required.

Morrison's method suggests that the total wave load is the sum of two components, the drag and inertial forces (Wheeler, 1969), where the inertial force is calculated by considering the fluid without viscosity accelerating uniformly and irrotational; while the drag component introduces a steady flow of a viscous fluid. The key to the hydrodynamic uncertainty problem is, therefore, to determine the distribution and hydrodynamic properties of the waves, to reach an accurate model.

The soil characterisation is an important issue for the foundations design, which requires a large investment to obtain the geotechnical properties and parameters of the site, reason for what remains a complicated task, as to reduce costs, the soil characterisation in the area is carried through a limited number of samples.

A standard has been developed by Bundesamt Für Seeschifffahrt Und Hydrographie (BSH), "Ground investigations for Offshore Wind Farms", to accomplish a ground investigation programme for the planning and construction of offshore wind turbines, to meet the requirements of (DNV, DNV-OS-J101: Design of Offshore Wind Turbine Structures, 2010). But although this standard helps to reduce uncertainties in the ground investigation process, it demands the soil characterisation just at turbine sites, leaving the rest and major part of the wind farm area under the ignorance, when as it was mentioned before, this is leading to rise costs, as it keeps the uncertainty of not knowledge of soil conditions over the total area.

The seabed in the North and Baltic Seas is not a homogeneous volume of sediments but may be a highly heterogeneous body on local scale (BSH, 2008). Unlike other type of materials like steel or concrete, which properties present a small range of variability, the soil properties show a wide range, and they cannot be changed to fit the structure. Furthermore, it is not simple to make accurate measurements of its properties on the one part that is tested. These

can lead to a huge uncertainty on the geotechnical conditions without the proper methods.

The Marine Environmental Mapping Programme (MAREMAP) of the United Kingdom Natural Environment Council (NERC) was initiated in June 2010 to update the maps of the national marine areas, making use of available data such as the British Geological Survey's (BGS) database on seabed sediments collected in several surveys from 1967 to 2009, or surveying new areas. The marine maps generated at 1:250000 scale are already available online (BGS, 2014) (see figure 2), and they are working interpreting more and new data to launch a new map generations at 1:50000 scale.

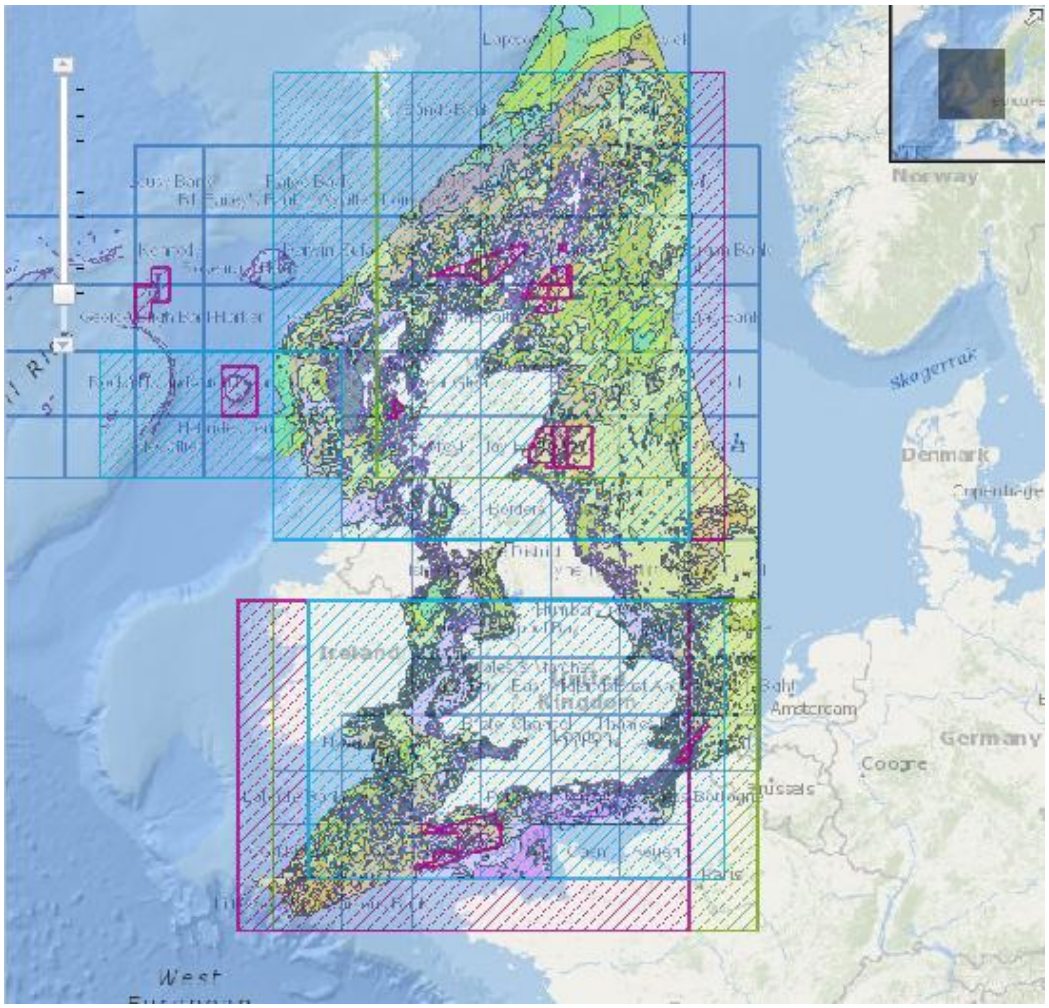

Figure 2: National area covered by MAREMAP

Source: (BGS, 2014)

In these maps we can see as the soil can change in hundreds of meters or keep homogeneous along kilometres, even with the large scale available. Figure 3 shows us an area where the soil changes between sandy gravel (left top) to sand (right bottom), through gravelly sand and slightly gravelly sand. These changes in the type of soil carry different soil properties due to their different composition.

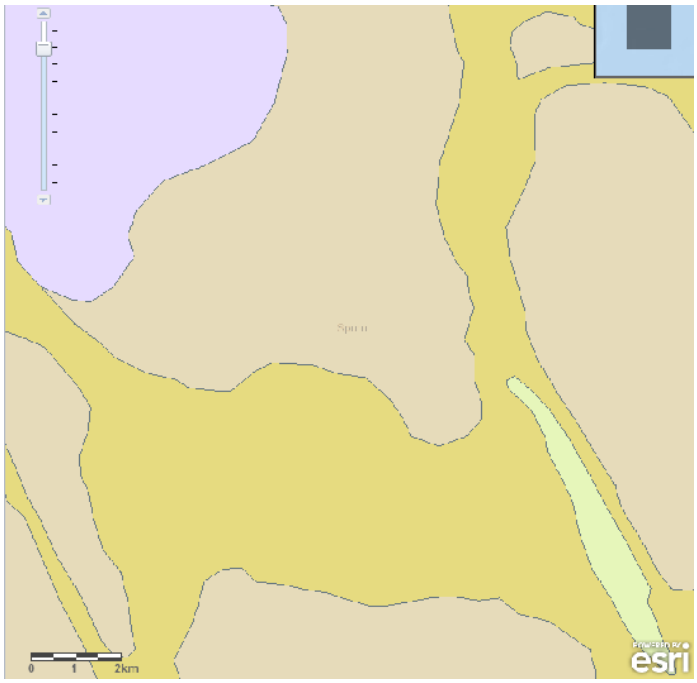

Figure 3: Random map selected

Source: (BGS, 2014)

Although these maps can be valuable to have a general overview of the sites, they have been generated in a traditional geological way (Lark, Dove, Green, Richardson, Stewart, & Stevenson, 2012), which means from sediment samples in addition to geophysical data (Cameron, et al., 1992; Gatliff, et al., 1994). More modern techniques strengthen the use of statistical methods for spatial prediction to map the seabed continuously, due these methods provide an account of the uncertainty in the predictions (Goovaerts, 2001).

This geographic information (GI) has not been a novelty from the marine environment, but another application of this methodology. A GI is the linking between locations and properties of those locations. Having properties in some

locations and needing to know the value of those properties on locations where are unknown, requires the use of spatial interpolation techniques.

A good soil characterisation allows adapting the foundations design to the soil conditions, reducing its uncertainty, but it is inevitable the existence of a certain grade of uncertainty. This leads us to considerate, besides the need to characterize the soil for all affected area, knowing if it is worth to take into account the soil properties, not just to design the foundations, but also to select the location of the wind turbines, from the soil conditions point of view.

1.2 Interpolation techniques in engineering

Spatial continuous data are significantly important in planning, risk assessment and decision making in environmental management. However, they are not always available and often difficult to acquire, especially for deep marine locations, where it can involve an expensive task. The environmental data is collected from field surveys typically made on point locations, but spatial continuous data over the region of interest are increasingly required to make confident and justified decisions (Collins & Bolstad, 1996; Hartkamp, De Beurs, Stein, & White, 1999).

Spatial interpolation techniques aim to estimate a continuous surface based on irregularly distributed data. That surface represents the value of the variable under study at any location over the region. The main issue in spatial interpolation is how to select an appropriate method to fit the dataset (Burrough & Mcdonnell, 1998).

Through the years, many techniques have been developed for different variables (Zhou, Guo, Ho, & Wu, 2007). Many factors such sample size, sampling design or the nature of the data may affect the estimation of a spatial interpolator, but there are not findings about how they can affect the performance of the interpolation (Li & D. Heap, 2008).

In geostatistics, there are two different methods according to the number of involved variables in the prediction; the univariate methods are the ones not able to use secondary information, while multivariate methods are able to make

use of it and then predict more than one variable at the same time. By other features they can be classified into exact vs. inexact, deterministic vs. stochastic or gradual vs. abrupt.

Estimations of almost all the spatial interpolation methods can be expressed as weighted averages of data:

$$\hat{y}(\boldsymbol{x}) = \sum_{i=1}^{n} \lambda_i y(x_i)$$

where $\hat{y}$ is the estimated value of the variable under study at the point of interest $\boldsymbol{x}$, y is the measured value at the sample point x_i, λ_i is the related weight to the sample point and n is the number of sample points for the estimation (Webster & Oliver, 2001).

Numerous methods have been developed for spatial interpolation. According to (Li & D. Heap, 2008), the used methods on environmental studies can be classified into three categories, geostatistical, non-geostatistical and combined methods. Geostatistical methods are those ones which provide statistical tools to incorporate the spatial coordinates of observations in data processing (Mabit & Bernard, 2007), where all samples are dependent from one another. However, non-geostatistical methods assume that there is not a spatial correlation among the sample data (Rouhani, Srivastava, Desbarats, Cromer, & Johnson, 1996).

Based on the conclusions obtained from 51 studies, kriging (geostatistic), inverse distance weighting (non-geostatistic) and cokriging (geostatistic) are the most commonly used methods on environmental sciences, including water resources, meteorology, ecology, agriculture, soil science and marine environmental science; where in general kriging methods perform better than non-geostatistical methods (Li & D. Heap, 2008).

It has been found the application of spatial interpolation techniques for characterization of the seabed. (Verfaillie, Lancker, & Meirvenne, 2006) compared linear regression and kriging with the version kriging with an external

drift to interpolate the variable median grain-size of the sand fraction at the Belgian Continental Shelf, where sandbanks and swales impose a high-spatial variability. Their study showed twice largest linear regression error than kriging.

(Li, Heap, Potter, Huang, & Daniell, 2011) compared 14 interpolation methods to predict the mud content across the southwest Australian margin from collected point sampling, incorporating as well secondary information such as bathymetry, distance to coast, slope or geomorphic province. It was found that a combined method was the most robust for this variable, random forest and kriging.

(Lark, Dove, Green, Richardson, Stewart, & Stevenson, 2012) illustrated the mapping of seabed sediment texture classes from the UK Continental Shelf by co-kriging methodology.

1.3 Aims & Objectives

The aim of this study is the characterization of the seabed, predicting the soil properties over the total affected area by a wind farm from data sample point observations, to reduce the project cost, reducing the uncertainties in the design. If we achieve to reduce the amount of data points under the number of installed wind turbines, the cost for the site investigation will be reduced; because the works will take less time, since the amount of data used have been the number of wind turbines, to date. Therefore, the soil characterization has to use the least amount of data as possible to reduce the site investigation cost.

In a typical offshore wind energy project, the cost of the foundations supposes the 21% of the total cost (RESCO, 2014). Keeping in mind the need of reduction the LCOE and taking into account the foundation design is based on the geotechnical conditions, is reasonable thinking about changing part or the entirety of the wind turbine locations to more strength sites, in order to reduce the necessary foundation cost and then reduce the LCOE. Although we cannot forget the wind source is not everywhere.

Dispersion shows that when wind turbines are spread over a larger area, the chance of optimal wind for energy production is larger than when wind turbines

are placed together in a small area (Van Assen, 2012). Besides, now the wind turbine locations are not where the wind gust is higher, but where the energy production covers the demand, in order to not need a storage system. So, as there is not a unique optimal location for the wind farm, we could introduce the request of optimal soil conditions in the decision making of the optimum location for the OWT and then also reduce the foundations cost. At the same time the demand is covered, also the energy cost can be reduced and meets the target.

This paper aims to address the issues set above, through employing approximation methods to 'map' a potential area of deployment of a wind farm, looking into the impact that reduction in sample points may have to the prediction results. Further, the impact of installation of a unit in locations with different geotechnical features is discussed in order to illustrate how the foundation design efficiency can influence the structural performance of structures.

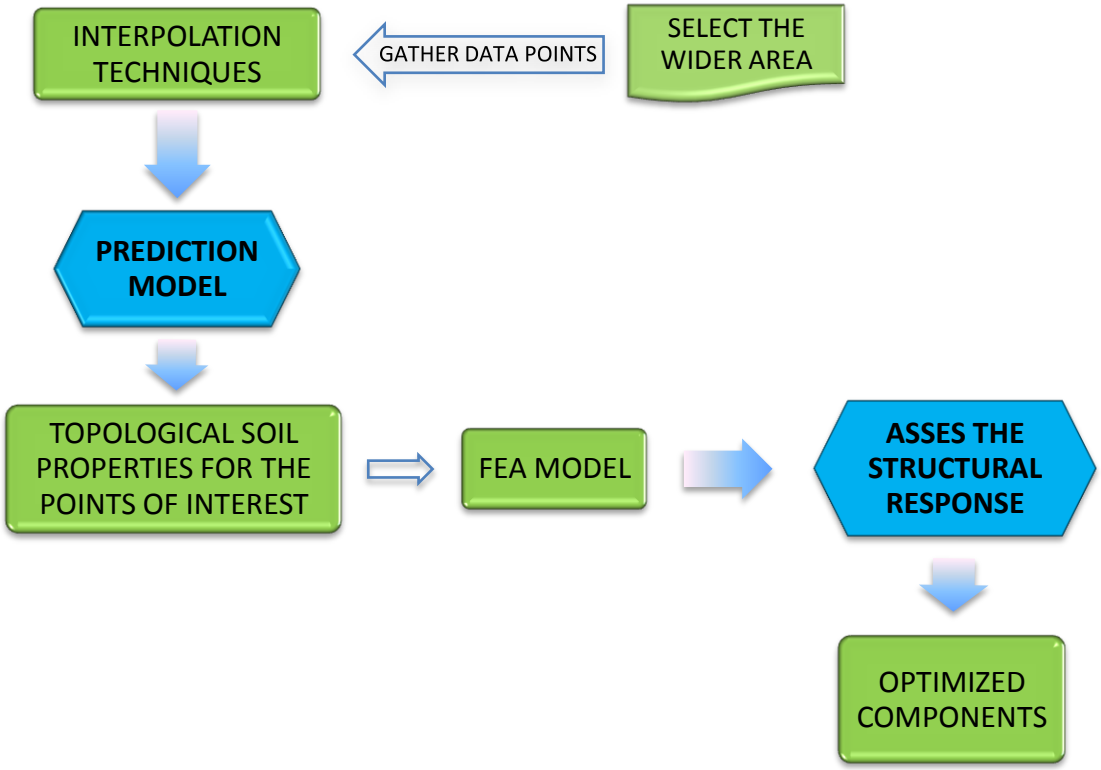

The flowchart set above shows the process that has been followed in this study. Once the soil properties are known in all the area under study, a finite element analysis is carried out to design wind turbine foundations for different locations inside the area, with different geotechnical characteristics. The different foundations are assessed to compare the geotechnical influence on its design, and then its influence on the total cost.

2 MODELLING OF GEOTECHNICAL CONDITIONS USING INTERPOLATION METHODS

The main objective of this study is to employ tools to determine the soil properties over the entire potential area of the wind farm deployment, just with the soil properties measured at a limited number of points. Although soil properties seem to show a random variability, it has been observed that close points to each other have similar characteristics (Webster, 1985). Due to this spatial dependence, classical statistic is not capable to analyze this kind of variable, as the data are assumed measured independently (Warrick, 1998).

Interpolation methods allow calculating the unknown values of any variable at points of interest by referring to the information of neighbouring points (Yang, Kao, Lee, & Hung, Twelve different interpolation methods: a case study of surfer 8.0, 2012). The variables in this research will be any necessary soil property to characterize the seabed of the wind farm.

Commonly, interpolation methods have been used in the fields of water resources, mathematics, ecology, petroleum engineering (Li & D. Heap, 2008). Further, applications can be found on mapping soil properties for geotechnical purposes as can be found in (Karydas, Gitas, Koutsogiannaki, Lydakis-Simantiris, & Silleos, 2009; Zandi, Ghobakhlou, & Sallis, 2012; Kazemi Poshtmasari, Tahmasebi Sarvestani, Kamkar, Shataei, & Sadeghi, 2012); but these geotechnical mapping applications are mostly found with environmental or agricultural objectives. However, this research aims to introduce it in the structural design for wind turbine installations.

2.1 Interpolation methods

The result of the prediction through approximation methods is a map which specifies the value of the variable at any location, which means to convert data from point observations to continuous map (Karydas, Gitas, Koutsogiannaki, Lydakis-Simantiris, & Silleos, 2009). Selecting of the most appropriate interpolation method is a crucial decision, since different methods can result in

different outcomes (Zandi, Ghobakhlou, & Sallis, 2012) as will be discussed later on the relevant section.

For this study two different methods are employed for soil characterization, in order to benchmark their accuracy and efficiency. As we could see in the previous section, kriging has been used several times to interpolate variables to characterize the seafloor. Kriging and also Radial Basis Functions (RBF) are two well-known spatial interpolation techniques (Zandi, Ghobakhlou, & Sallis, 2012) and are found to perform well comparing obtained results to actual quantities (Yang, Kao, Lee, & Hung, 2012).

2.1.1 Radial Basis Functions

Radial basis function was first introduced by the geodesist Roland Hardy in 1968. We can find applications from medical purposes (Carr, Fright, & Beatson, 2002) to engineering problems in fields as solar energy (Mohandes, Balghonaim, Kassas, Rehman, & Halawani, 2000) or tidal energy (Yin, Zoua, & Xu, 2013), among others.

RBF works given data sites ξ in n dimensions, where $\xi \in \mathbb{R}^n$ and function values that we know are $f_\xi = f(\xi) \in \mathbb{R}$. What this method will seek is an approximation $s: \mathbb{R}^n \to \mathbb{R}$ to the function $f: \mathbb{R}^n \to \mathbb{R}$.

To approximate s to f, it is explicitly required $s|\Xi = f|\Xi$, where $\Xi \subset \mathbb{R}^n$ is the set of data sites, which means the approximation function will have the same value of the data over the sample data locations.

This is a diverse group of interpolation methods, in which five deterministic interpolation techniques are part of it: thin-plate spline, spline with tension, completely regularised spline, multi-quadric function and inverse multi-quadric function (Zandi, Ghobakhlou, & Sallis, 2012; Sarra & Kansa, 2009). The obtained results are quite similar for all of them (Burrough & Mcdonnell, 1998), but according to (Yang, Kao, Lee, & Hung, 2012), multi-quadric method is considered the best.

A RBF is a function based on a scalar radius:

$$\phi(r) = \phi(\|x - x_i\|)$$

where radius, $r = \|x - x_i\|$, represents the radial distance, between the predicted point and the data ones, taking into account that x represents the location of the predicted point, and x_i represents the data point locations.

For multi-quadric method, the expression of the basis function is:

$$\phi(r) = \sqrt{1 + \frac{r^2}{\sigma^2}}$$

where σ is the shape parameter, which is the average distance between data points. Normally, the radial basis function method accuracy increases with σ (Bayona, Moscoso, & Kindelan, 2011).

Given this information, the approximant is created by the sum:

$$s(x) = \sum_{\xi \in \Xi} \lambda_\xi \phi(r) \qquad x \in \mathbb{R}^n$$

where λ_ξ are scalar parameters. But sometimes the existence of the interpolation just can be guaranteed by a small variation of this function, adding polynomials to s. Therefore, the approximation function has the form:

$$s(x) = c_0 + c_1 x + \sum_{\xi \in \Xi} \lambda_\xi \phi(r) \qquad x \in \mathbb{R}^n$$

with real coefficients c_0, c_1, and λ_ξ. This coefficient values will be calculated by forcing the function to meet the real values at the prediction points and taken into account this two conditions: $\sum_{i=1}^{n} \boldsymbol{\lambda_i} = \mathbf{0}$ and $\sum_{i=1}^{n} \boldsymbol{\lambda_i x_i} = \mathbf{0}$, while n is the amount of sample points.

2.1.2 Kriging

The mining engineer Danie Krige developed the spatial interpolation technique, kriging, to predict the mineral concentration in the ground. Geostatistical interpolation by kriging is long-established (Matheron, 1963; Journel &

Huijbregts, 1978; Webster & Oliver, 2001) and has been applied on environmental sciences including hydrology (Zimmermann, Zehe, Hartmann, & Elsenbeer, 2008), agronomy (Bishop & Lark, 2007) and soil survey (Burgess & Webster, 1980), among others. Afterwards it has been also used with geotechnical purposes to solve other environmental problems (Dai, Zhou, Lv, Wang, & Liu, 2014; Chica-Olmo, Luque-Espinar, Rodriguez-Galiano, Pardo-Igúzquiza, & Chica-Rivas, 2014; Gong, Mattevada, & O'Bryant, 2014).

This method is a linear combination of radial basis function, with centres on data points, where μ is a constant term from which prediction starts that will move with some deviations.

$$y(\boldsymbol{x}) = \mu + Z(\boldsymbol{x})$$

where **x** is an n-dimensional vector (n design variables) and $Z(\boldsymbol{x})$ represents a local deviation from the global model. The sample points are interpolated with the Gaussian random function as the correlation to estimate the trend of the stochastic processes. The correlation between $Z(\boldsymbol{x^i})$ and $Z(\boldsymbol{x^j})$ is related to the distance between the two corresponding points, but instead of use the Euclidean distance, it is used this expression:

$$d(\boldsymbol{x^i}, \boldsymbol{x^j}) = \sum_{\boldsymbol{k=1}}^{\boldsymbol{n}} \theta_k \left| \boldsymbol{x^i_k} - \boldsymbol{x^j_k} \right|^2$$

which weights different each design variable; where θ_k $(0 \leq \theta_k \leq \infty)$ is the k_{th} element of the correlation vector parameter $\boldsymbol{\theta}$. By using this expression for the distance and the Gaussian random function, the correlation between both points is:

$$corr[Z(\boldsymbol{x^i}), Z(\boldsymbol{x^j})] = e^{-d(\boldsymbol{x^i}, \boldsymbol{x^j})}$$

Then Kriging predictor is:

$$\hat{y}(\boldsymbol{x}) = \hat{\mu} + \mathbf{r}'^{\mathrm{T}} \mathbf{R}^{-1} (\mathbf{y} - \mathbf{1}\hat{\mu})$$

where $\hat{\mu}$ is the estimated value of μ, **R** denotes the nxn matrix whose (i, j) entry is its correlation, **r** is vector whose i_{th} element is $r_i(\boldsymbol{x}) \equiv corr[Z(\boldsymbol{x}), Z(\boldsymbol{x^i})]$ and

$\boldsymbol{y} = [y(x^1), \ldots, y(x^n)]$. The complete derivation of the predictor can be found in (Koehler & Owen, 1996).

The unknown parameter to construct Kriging model is $\boldsymbol{\theta}$, which can be estimated by maximizing the likelihood function presented in (Jeong, Murayama, & Yamamoto, 2004)**.**

2.2 Case study data set

Taking into account that the soil-structure interaction method used will be Winkler method, which will be justified later; the necessary soil properties are Young's modulus and Poisson's ratio.

The Young's modulus, E_s, is the property of the soil which describes its stiffness. It is a measure of the ability of the soil to resist changes in length when is under tension or compression, which has a large range of variation. For granular soils we can find a range between 7 to 320 MPa, and for cohesive soils from 0.35 to 80 MPa (Kezdi, 1974; Prat, Bisch, Millard, Mestat, & Cabot, 1995).

Poisson's ratio, ν_s , is the ratio of transverse to longitudinal strain under an applied stress. When rigidity is zero, Poisson's ratio is 0.5 (Hamilton, 1979), but most natural sediments and rocks have enough rigidity, so Poisson's ratio uses to be less than 0.5 (Hamilton E. , 1971). We can understand that if the soil would be extremely rigid, Poisson's ratio would reach the value of zero, therefore Poisson's ratio can vary from 0 to 0.5.

Based on this, a typical data map has been generated for each property; representing by contours the value of the properties at every point in the area. See figure 4.

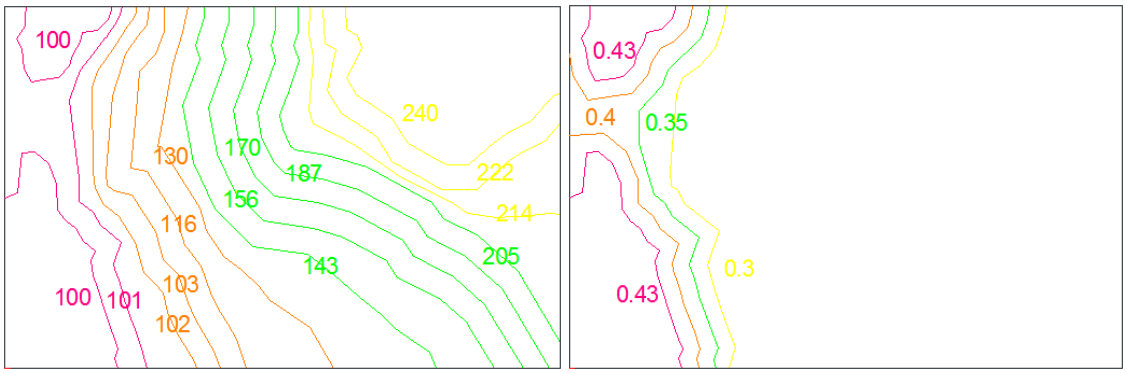

Figure 4: Real contours for Young's modulus [MPa] and Poisson's ratio respectively

As all the operational wind farms in UK cover approximately an area between 4 (Scroby Sands) and 146 km^2 (Greater Gabbard) (4COffshore, 2014), but most of them are under 40 km^2, it has been selected a middle area of 15 km^2 (5000 m x 3000 m). This assumption makes us unable to extrapolate the results from this study in terms of numerical values; meanwhile it helps us to determine the accuracy of the method.

The soil properties are considered constant with depth to simplify the calculations, although in reality they are not. In any case, the methodology developed herein can be extended to account for the depth coordinates of spatial points.

As the aim of this research requires that the amount of data is the minimum as possible, four sets of data have been selected with 7, 15, 20 and 96 sample points in total, which will be the input in the prediction methods (see figure 3). We will compare their results and select the minimum.

It is recommended that sampling is randomly distributed in the space (Li & D. Heap, 2008), because this is expected to lead to higher accuracy in the prediction; although the data distribution for 96 points is uniform as it would not differ too much.

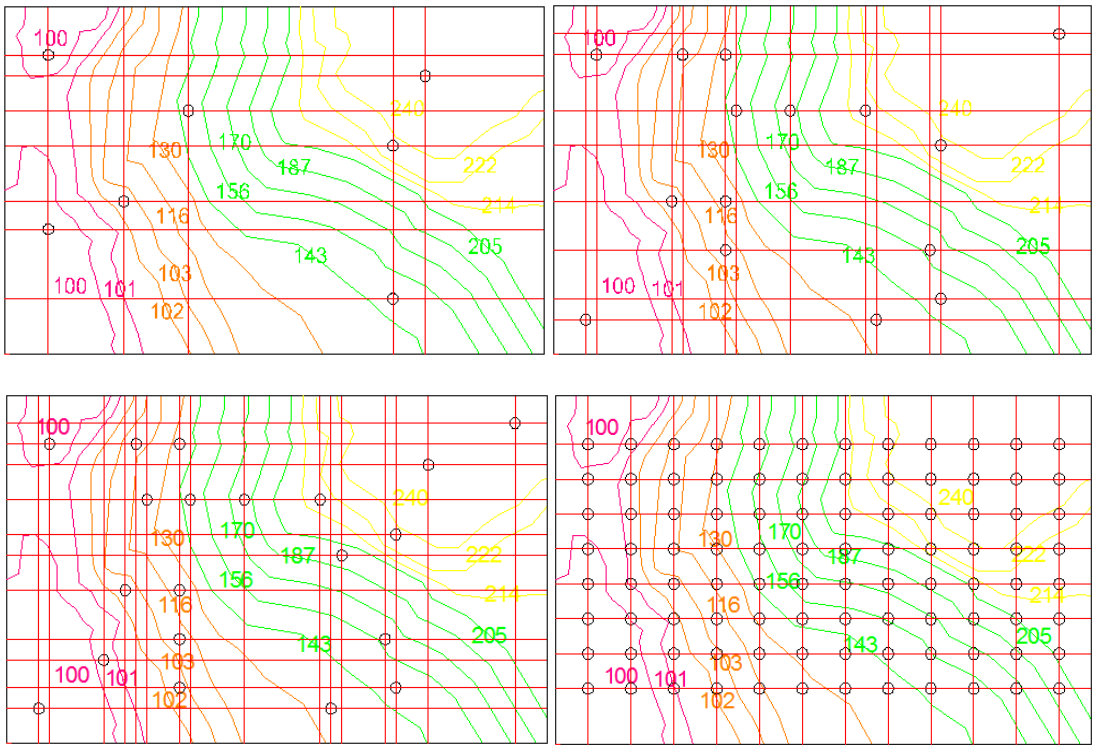

Figure 5: Distributions for 7, 15, 20 and 96 points

These are the distributions for the young's modulus, which will be exactly the same for the Poisson's ratio.

2.3 Prediction models and their validation

As not all prediction methods give the same results, to find the optimal choice from which have been proposed, it is necessary to measure the accuracy of each method.

According to (Krivoruchko & Gotay, 2003), the accuracy is measured by the Mean-Squared Error (MSE) and one measure of effectiveness is Goodness-of-Prediction Estimate (G), both necessary to assess the prediction.

The MSE is given by the equation:

$$MSE = \frac{1}{n}\sum_{i=1}^{n}(|z(x_i) - \hat{z}(x_i)|)^2$$

where $z(x_i)$ is the measured value at data survey on location i, $\hat{z}(x_i)$ is the predicted value at location i and n is the sample size. A small value of MSE indicates more accurate prediction (Karydas, Gitas, Koutsogiannaki, Lydakis-Simantiris, & Silleos, 2009).

And G might be calculated as:

$$G = \left(1 - \frac{\sum_{i=1}^{n}(z(x_i) - \hat{z}(x_i))^2}{\sum_{i=1}^{n}(z(x_i) - \bar{z})^2}\right) \cdot 100$$

where $z(x_i)$ is the measured value at data survey on location i, $\hat{z}(x_i)$ is the predicted value at location i, $\bar{z}$ is the sample mean and n is the sample size. A G value of 100% indicates a perfect prediction (Karydas, Gitas, Koutsogiannaki, Lydakis-Simantiris, & Silleos, 2009).

2.4 Results

2.4.1 Evaluation of the prediction maps

The outcomes from the prediction methods have been evaluated by MSE and G, which results are shown in figures 6 and 7.

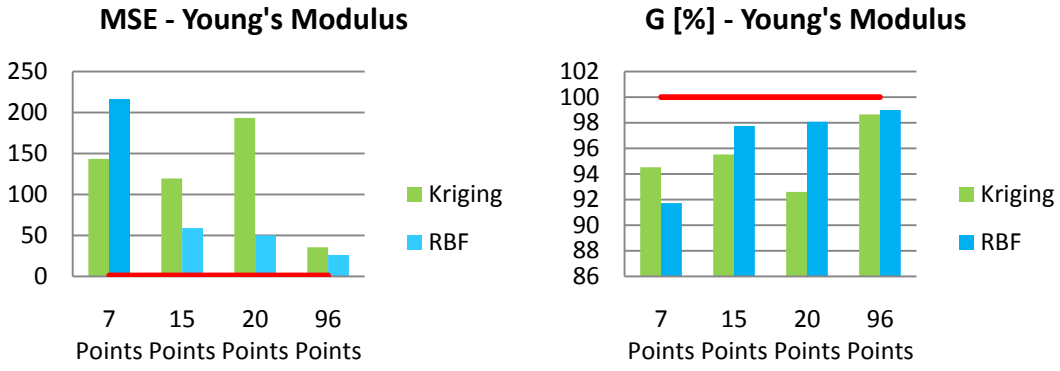

Figure 6: Evaluation of the Young's modulus prediction

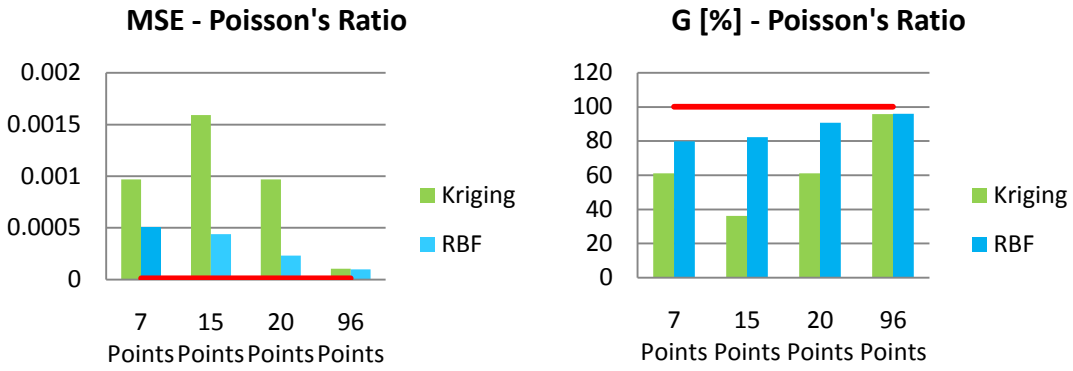

Figure 7: Evaluation of the Poisson's ratio prediction

In last two figures it can be seen represented by a red line the optimum value of both the Mean-Squared Error and the Goodness-of-Prediction Estimate.

Observing the obtained results for the Young's modulus variable, we see as not for all data predictions the same approximation method gives better results. In general, radial basis function offers better results, with MSE values closer to zero and G values closer to 100%, but in the case of 7 sample points the accuracy is the smallest one with the bigger generated error. Nevertheless for Poisson's ratio variable, RBF gives better results all the time, with higher accuracy and smaller error.

It attracts our attention the fact that not bigger amount of samples offer better results by Kriging method, as in Young's modulus prediction with 20 sample points the accuracy of the results is worst than for 7 or 15; and in Poisson's ratio it happens the same with 7 sample points, which offer better results than 15 samples and almost the same as 20.

In order to make a visual examination of both methods, it has been represented in the next figures the real data (red surface) against the measured values.

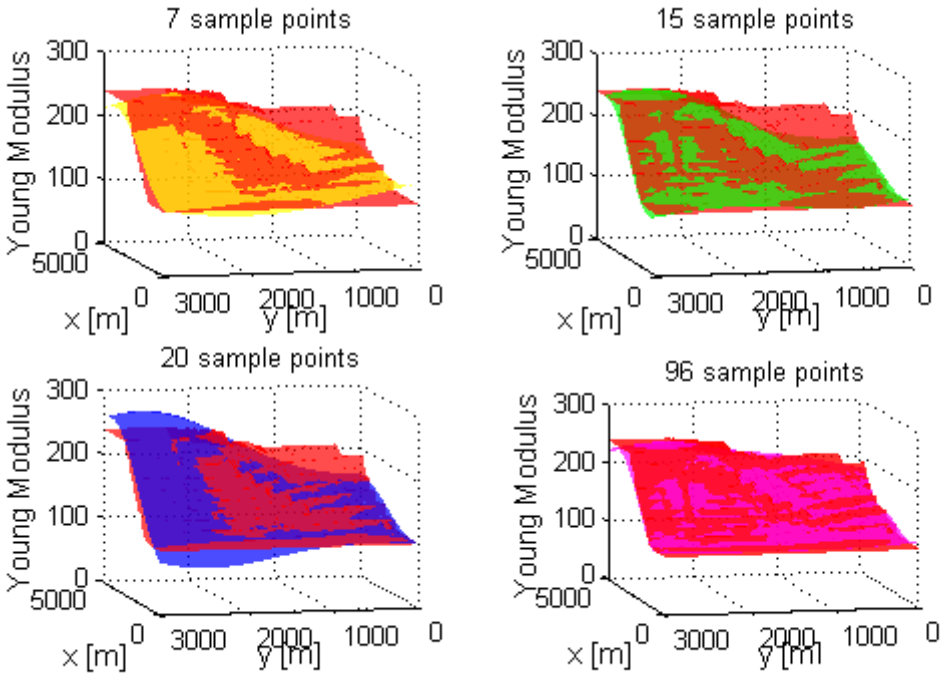

Figure 8: Actual vs. Measured Young's Modulus data – Kriging method

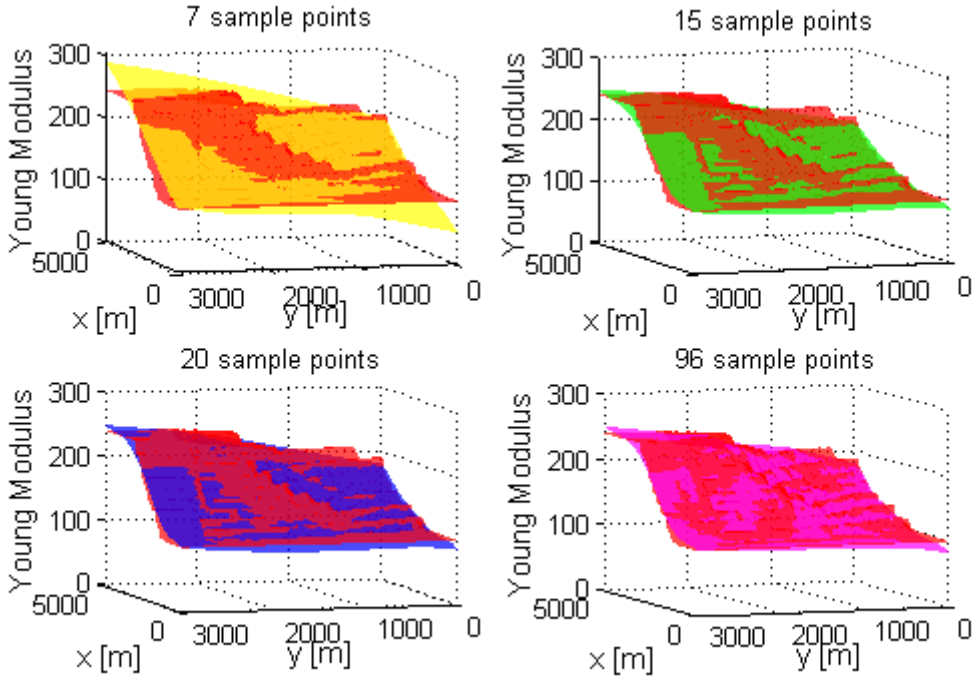

Figure 9: Actual vs. Measured Young's Modulus data – RBF method

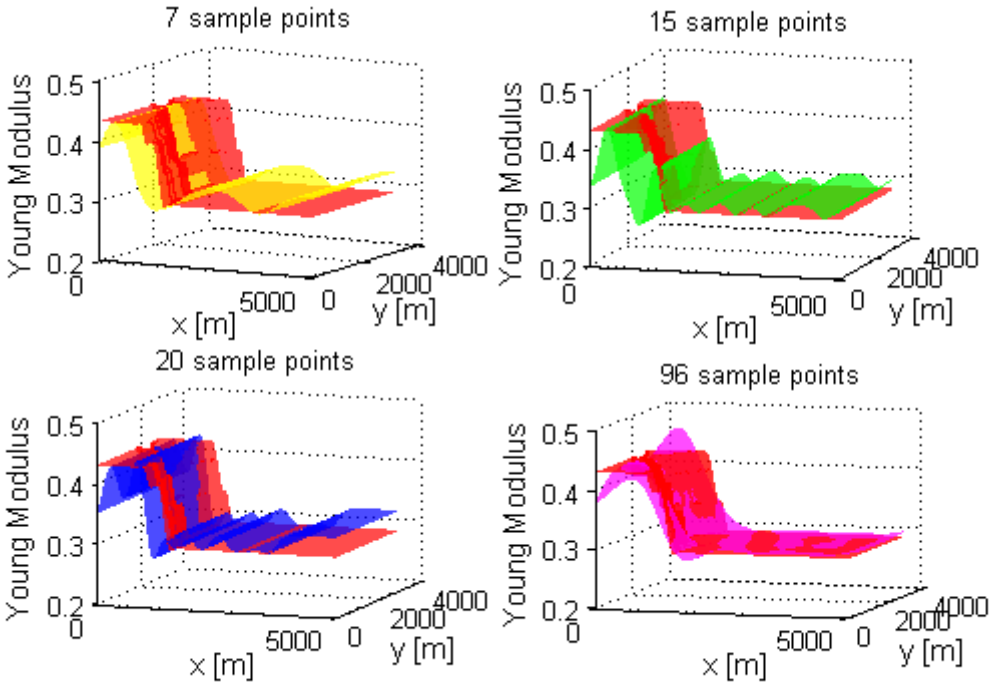

Figure 10: Actual vs. Measured Poisson's Ratio data – Kriging method

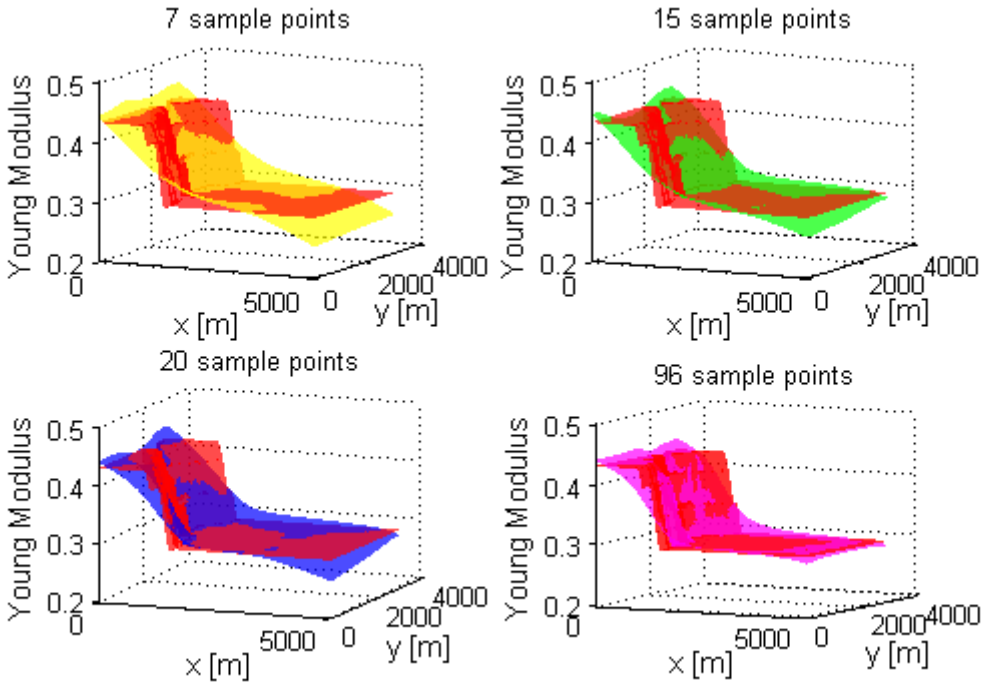

Figure 11: Actual vs. Measured Poisson's Ratio data – RBF method

Comparing the visual representations of the results in three dimensions (3D), Young's modulus graphs by Kriging method confirm as the prediction with 20 sample points is less accurate than the rest and the same for Poisson's ratio variable which results with 7 samples give better accuracy than with 15 or even 20; while RBF method performs better the real data when higher amount of samples are available.

2.4.2 The best prediction method

The method selection is based on how the prediction is able to perform the reality, which is the real value of the variables, based on the validation process. From our evaluation we are looking for the prediction with the minimum MSE and the G value closer to 100%, which will mean it is the most accurate prediction between which we have. But at the same time, it is compulsory for this research to meet the requirement of fewer amount of samples for the prediction. So, based on this evaluation, the selected method as the best for both variables in this case is radial basis functions performed with 20 sample points, because this reaches at least a 90% of effectiveness.

The amount of data is 1.33 samples/km^2, which will be compared with the amount of installed wind turbines. Thus, we will have to assume as good the MSE values, which are not minimum because as it is obvious a greater amount of data gives less MSE, for the selected method.

We cannot conclude that RBF is the best method, because there is no general best prediction method, as each one can be the best for a specific variable (Isaaks & Srivastava, 1989); that is the reason to use at least two different methods, to compare their results and find the best one for our case. But although we cannot say RBF is the best method, observing its behaviour along the predictions, it gives in general better results than Kriging, with higher accuracy as bigger amount of sample points available; its performance tells us that it is better method than Kriging, although in one prediction with fewer samples might give better results.

2.4.3 Prediction maps of soil properties

Based on the selected method as the best one for our soil properties (20 sample points by RBF), the prediction maps are:

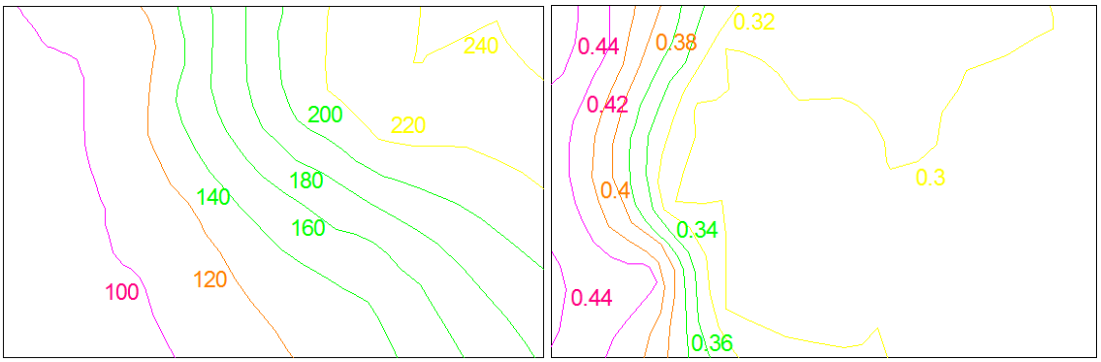

Figure 12: Young's modulus [MPa] and Poisson's ratio prediction, respectively

Putting together both soil properties and according to (Kezdi, 1974; Prat, Bisch, Millard, Mestat, & Cabot, 1995; Hamilton E. L., 1979; Hamilton E. , 1971), we can identify three different types of soil: clay, dense sand and very dense sand, as it can be seen in figure 13.

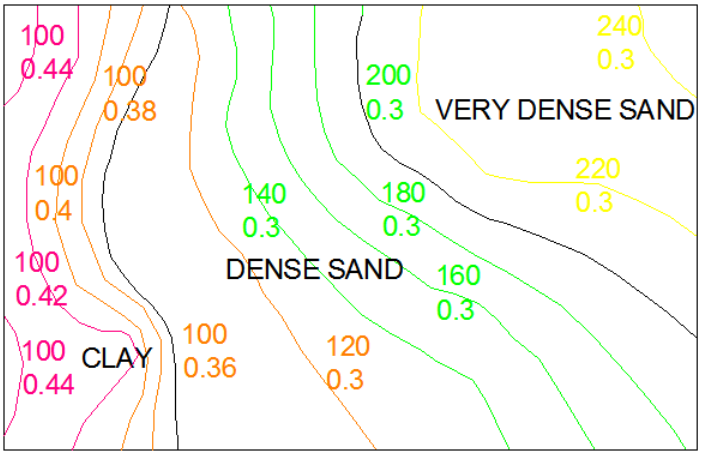

Figure 13: Soil type identification

3 DESIGN OF FOUNDATIONS FOR WIND TURBINE MONOPILE STRUCTURES

3.1 General

The foundation comprises a set of components which aim to transfer the loads from the structure to the soil. They have to redistribute the loads in order for the settlement and the stresses do not exceed the allowable maximum. The design of foundations requires selecting the appropriate geometry for the selected foundation type, according to the conditions that the foundation has to accomplish to ensure the safety and functionality of the structure.

There are five different main offshore wind turbine support structures, monopile, gravity, tripod, jacket and floating structures (Buren & Muskulus, 2012):

- The monopile foundations consist on a tubular steel structure to support the tower, either directly or through a transition piece. This tube extends down the water, into the soil, with a depth limitation up to 25 m (DNV, 2010).
- The gravity type support structures are a concrete flat based structure which width is adjusted to suit the soil conditions. Its design requires a steel or concrete shaft for connection with the wind turbine tower. These types of structures are suitable for sites with firm soils or those with a minor need of improvement on water depths up to 25 m (DNV, 2010).
- The tripod foundation consists on a tripod structure anchored to the soil either by piles or suction buckets, depending on the soil conditions. This support structure suits well on water depths between 20 to 50 m (DNV, 2010).
- The jacket structures or lattice towers, consist on a four-legged tower interconnected with bracings. At the seabed the structure is connected to piles, one per leg, to gain stability of the structure. These structures are recommended for water depths between 20 to 40 m (DNV, 2010).
- The floating systems for wind turbines consist on a floating platform with enough buoyancy to support the wind turbine weight and its own. These are a new generation of support structures for the offshore wind turbines

to reach deeper waters, as they are suitable for depths greater than 50 m (Lefebvre & Collu, 2012).

The majority of the operational and decommissioned offshore wind farms in the UK are at locations where water depths do not exceed the 30 m (Higgins & Foley, 2014). The next expected step in the near future is to continue growing into further from shore and deeper site locations (Buren & Muskulus, 2012).

Monopile support structures have been used for the 96% of the commissioned offshore wind turbine foundations and the 4% remaining are jackets (Higgins & Foley, 2014). Although normally monopile foundations have been recommended for water depths up to 25 m, as they are the more developed and best well known, the cost of the support structure supposes less investment in the total cost than for the rest of the foundation types (Lozano-Minguez, Kolios, & Brennan, 2011); then paying more attention to the design, studies as (Scharff & Siems, 2013) demonstrates as monopile foundations can be used as support structures for wind turbines at deeper locations.

Then monopile support structures are selected for the study of this research.

3.2 Basis for analysis

Design of offshore structures is governed by relevant design standards, ie DNV-OS-J101 or DNV-OS-C101, which include provisions for derivation of reliable support structures. Design requirements include ultimate and fatigue limit states to be examined in order to assess structural resistance to the loads the structure should withstand.

3.2.1 Ultimate limit state assessment

For the comparative nature of the present work, a simplified approach has been adopted, by considering the ultimate resistance of each of the different geometries through estimation of the Von Mises stress combined with the verification of the maximum deflection for each different topology. Hence, when measured stress (σ_v) exceeds the yield strength of the material ($S_y = 355\ \mathrm{MPa}$), it is considered to have failed:

$$\sigma_v < \frac{S_y}{\gamma}$$

Where γ is the global safety factor to reduce the yield stress, which is obtained considering the equilibrium state between loads (L) and resistance (R):

$$\gamma_i \cdot L = \frac{R}{\gamma_M}$$

$$L = \frac{R}{\gamma_M \cdot \gamma_i} = \frac{R}{\gamma}$$

γ is the product between the material safety factor (γ_M) and the partial load safety factor (γ_i), which values are 1.15 and 1.35, respectively (British Standard, 2006), so $\gamma = 1.55$. This is the minimum safety factor to require to the structure.

On the other hand, as there is no official recommendation for the horizontal deflection, it has been selected a maximum allowable deformation up to 2% of the total length of the structure.

3.2.2 Fatigue limit state assessment

The fatigue is the degradation of the material caused by cyclic loading. As DNV-RP-C203 recommends, the fatigue analysis is based on S-N curves, where S is the fatigue strength and N the fatigue life, measured in number of cycles.

As the potentially sources of fatigue cracking are the joints, due to the stress concentration as they are discontinuities in the structure; the fatigue assessment is carrying on focus at the joints tower-transition piece and transition piece-pile. Based on the detail of these joints, the selected curves are D from the DNV-RP-C203 joint classification, in air and seawater, respectively.

This RP (recommended practice) points that for offshore structures significant damage occurs for $N \geq 10^7$cycles, so the requirement to meet by our structures is:

$$N < 10^7 \text{cycles}$$

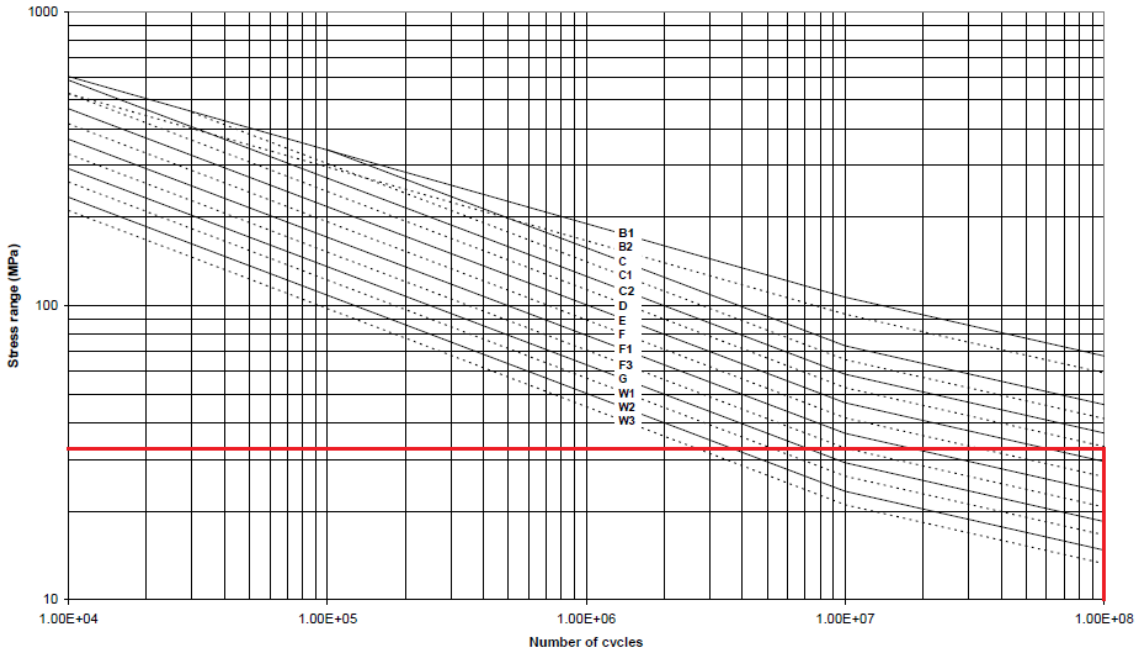

Figure 14: S-N curves in air

Source: DNV-RP-C203

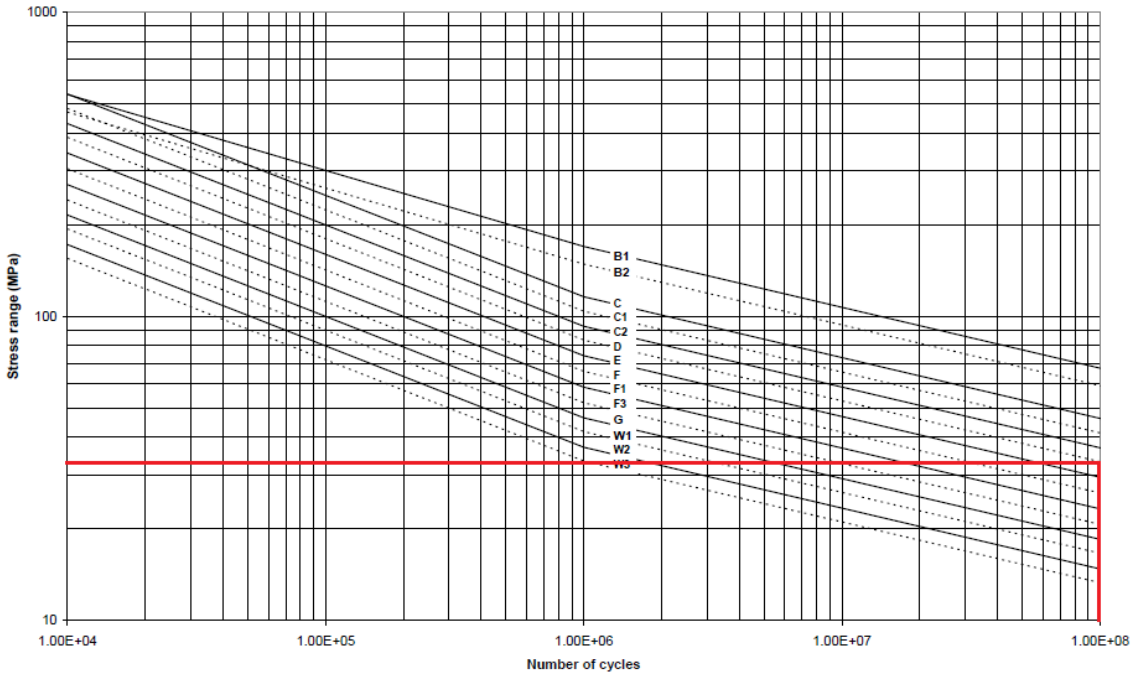

Figure 15: S-N curves in seawater

Source: DNV-RP-C203

Although these curves are different for each environment, as they have different slope, the maximum operational stress allowable, given by the maximum number of cycles is the same, 33.3 MPa.

The structure is able to withstand higher stresses, as it can be read in figures 14 and 15. We can see as a higher stress can be allowed, but the fatigue life of the structure would be shorter; this means those higher stresses must occur on temporary situations, when its number of repetitions is smaller, as it happens on the ultimate limit state.

3.3 Finite element model

3.3.1 Structural modelling

Displacements and corresponding stresses have been derived by using commercial Finite Element Analysis (FEA) tool ABAQUS CAE. Based on the geometry to be modelled, beam elements were employed with a mesh independence study on a generic case to illustrate the optimum mesh size that was later used in all cases.

The next figures show the stresses and displacements for different mesh sizes in the finite element analysis on a generic case. In figures 16 and 17 it can be seen as the results converge as the mesh size becomes smaller and we can be underestimating the stresses by selecting an inappropriate mesh size. From this study it is concluded the optimum mesh size is 0.1 m, from the point of view of the reliability of the results.

Figure 18 shows the mesh size against the corresponding number of elements for the analysis. We can see as for mesh sizes smaller than 0.1 m, the number of elements excessively increases. As the calculating time is related to the number of elements, greater amount of elements implies higher calculating time; so the mesh size 0.1 m offers reliability results without waste time.

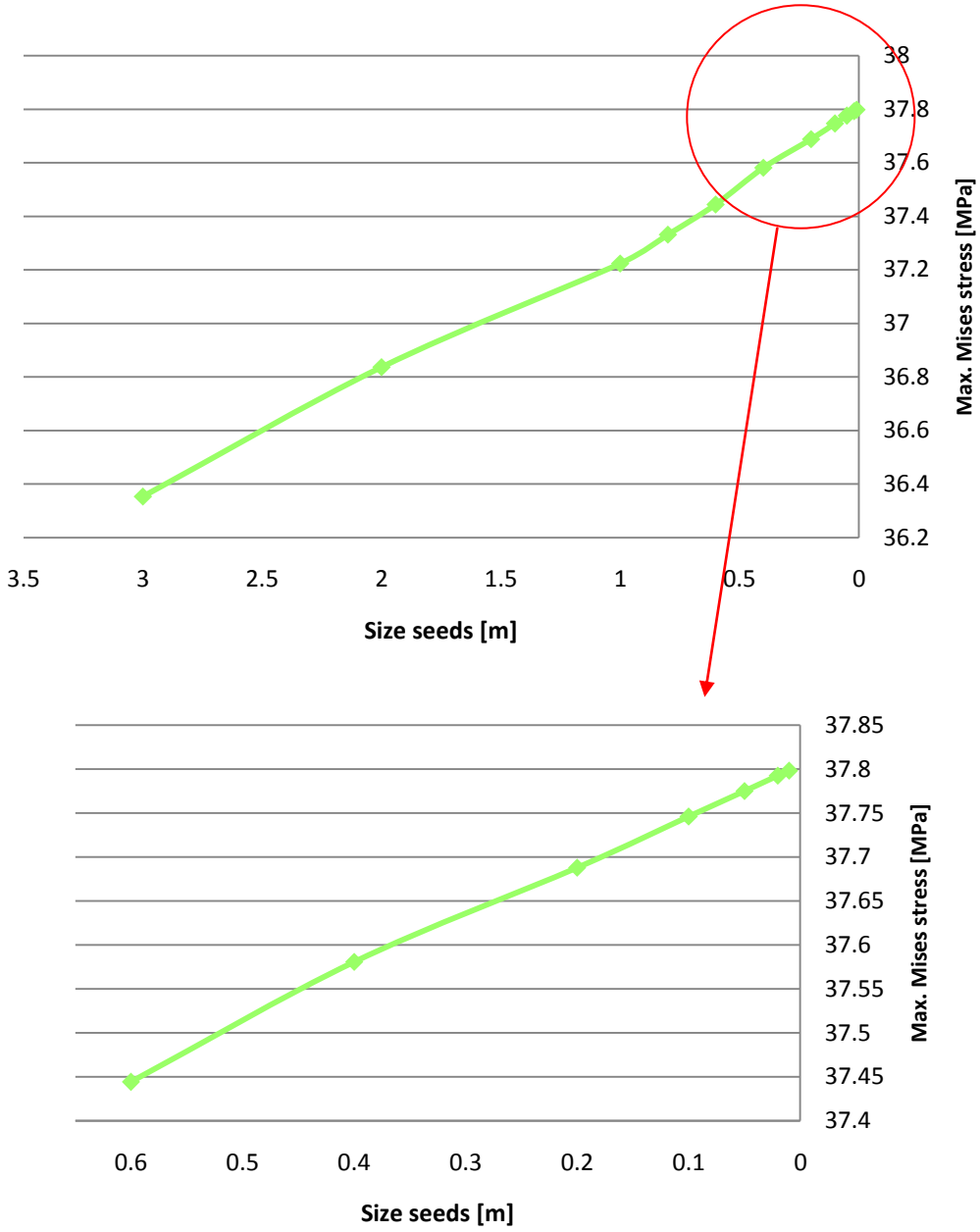

Figure 16: Maximum Mises stress vs. mesh size

Figure 17: Maximum displacement vs. mesh size

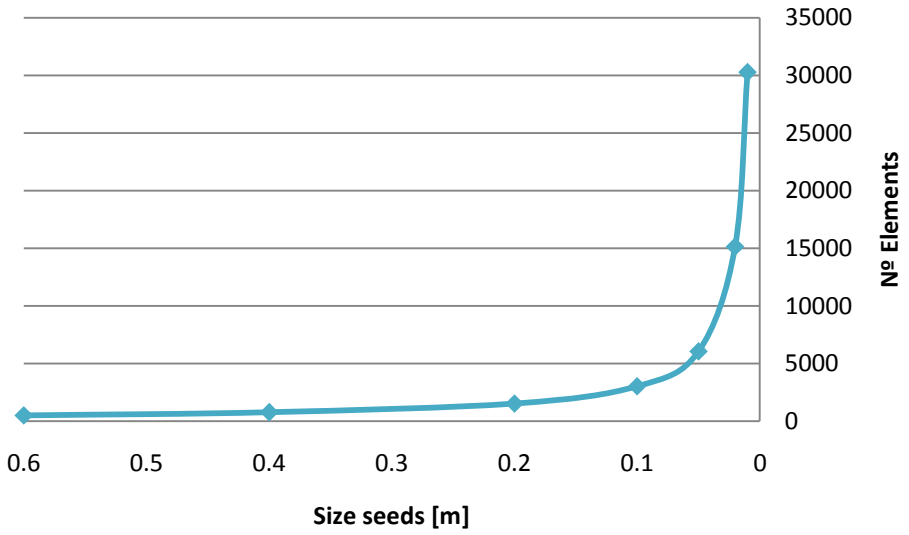

Figure 18: Number of elements vs. mesh size

3.3.2 Soil modelling

Considering that this is a soil-structure interaction problem, realistically modelling the boundary conditions become an issue of great importance. There are two generic approaches to model the soil-structure system (Hare & Harwood, 2013). The direct one models explicitly a volume of soil with the structure and gives a total solution with an only analysis. Other ones consist in

an indirect approach, as the soil is modelled with springs and dampers based on its properties.

The offshore standard DNV-OS-J101 recommends the p-y curves method, which is an indirect method, to introduce the realistic stiffness values for the soil, in the case of dynamic analysis of the system for pile foundations, following the recommendation from the American Petroleum Institute (API) code, which recommends the p-y method for the design of horizontal loaded piles.

This method models the soil reaction as localized nonlinear springs based on Winkler's method (Kikuchi & Kimura, 2007). The p-y curve represents the lateral soil resistance (p) expressed as function of lateral soil movement (y). It is based on test results of laterally loaded piles; its empirical formulation of the curves are different for different type of soils and depend on the pile diameter, the soil strength and the loading conditions, although other effects like layered soils or the space between piles is also considered (Chen & Duan, 1999).

Although the p-y method is the widely used (Heidari, Naggar, Jahanandish, & Ghahramani, 2014), it was developed for piles with diameters up to 2 m and as (Abdel-Rahman & Achmus, 2005) conclude, comparing the behaviour of larger monopiles by using p-y curves and a three dimensional numerical model, the p-y method underestimates pile deformations.

Direct methods like the three dimensional numerical model which gives the total solution based on a finite element analysis, where the soil is modelled as a big volume, enough for the structure does not affect its external edge, are more accurate, but at the same time require more calculation time.

In this research the performed analysis is just static, with the aim to obtain the structure deformations and the generated stresses under the different loading cases. Considering the steel is an elastic material, the relationship between the stress and the deformation is linear, so it is considered an indirect approach is enough for the purpose of this study.

As it was mentioned before, the indirect method p-y is the widely used and recommended from several industrial organizations, but at the same time it

cannot be used for monopile structures, as normally have a wider diameter. P-y method is based on Winkler's method, which ignores the global effect of a continuum, but allows us to model the soil-structure interaction for piles with diameter wider than two meters; for this reason it has been selected for this research.

Winkler method models the interaction from the soil over the structure by replacing the elastic soil medium by closely spaced and independent elastic springs (Winkler, 1867). The stiffness of these springs, also called modulus of subgrade reaction, is:

$$k_s = \frac{p}{y}$$

where p is the soil reaction on the structure per length unity and y is the deflection.

For the modulus of vertical subgrade reaction, k_{sv}, the elastic deformation under a circular area, which diameter is D, supporting a uniformly spread load, q, is:

$$y = \frac{Dq(1-\nu_s^2)}{E_s}$$

being ν_s the Poisson's ratio and E_s the elasticity modulus. And with the combination of the last two expressions, we have:

$$k_{sv} = \frac{E_s}{D(1-\nu_s^2)}$$

The Winkler model can be simplified by means of finite number of springs of stiffness K, instead of the springs bed (Aysen, 2005), which expression is:

$$K = ak_{sv}$$

Where *a* is the contact area corresponding to a single spring.

On the other hand, to the modulus of horizontal subgrade reaction, k_{sh}, we do not have a only expression, but we will have a expression to every soil type.

For granular soils, k_{sv} is considered directly proportional to depth:

$$k_{sh} = n_h\, x$$

Where n_h is the constant of horizontal subgrade reaction and *x* is the depth. n_h depends on the soil damp and its density. The suggested values are:

Relative density of sand	**Loose**	**Medium**	**Dense**
Range of values of A	100-300	300-1000	1000-2000
Adopted values of A	200	600	1500
Dry or moist sand, values of n_h	7	21	56
Submerged sand, values of n_h	4	14	34

Table 1: n_h values in tons/cu

Source: (Terzaghi, 1955)

In this case, the stiffness for each spring is:

$$K = L\, k_{sh}$$

Where L is the length associated to each spring.

For cohesive soils, k_{sv} is:

$$k_{sh} = \frac{\overline{k_h}}{5\, D}$$

Where $\overline{k_h}$ is the constant of horizontal subgrade reaction and *D* the pile diameter. The constant of horizontal subgrade reaction in this case depends also on the damp and density of the soil and the suggested values are:

Consistency of clay	Stiff	Very stiff	Hard
Range of q_y, tons/sq. ft	1-2	2-4	> 4
Range for k_{s1}	50-100	100-200	> 200
Proposed values	75	150	300

Table 2: $\overline{k_h}$ values in tons/cu

Source: (Terzaghi, 1955)

Finally, the stiffness for each spring in cohesive soil is:

$$K = D\ k_{sh}$$

As it was mentioned previously, Winkler method ignores the global effect of a continuum, it idealizes the soil assuming that the deflection of the soil at any point on the surface is directly proportional to the stress applied at that point and independently of any stress applied at other locations, which is not normally true, because deflection will occur also within a limited region outside the loaded area (Selvadurai, 1979). So, this limits its application to soils with slighted cohesion or transmissibility of applied loads. But its simple expression allows applying it frequently to flexible elements, like in (Zhong & Huang, 2013).

In this case it has been used the simpler model of Winkler, replacing the soil by lateral translational springs 10 m spaced along the pile length relating horizontal displacement at a particular depth, and another one relating the toe resistance. Other more sophisticated and accurate versions of Winkler method add springs relating the rotation along the foundation periphery as (Gerolymos & Gazetas, 2006) does. Based on this version, in order to make the model more accurate it was limited the rotation of the pile according to its torsional resistance, as if it would have been applied a rotational spring. This torsional resistance (K_{tor}) is calculated as (Bowles, 1996) indicates, which is also:

$$K_{tor} = \frac{M_{tor}}{\theta}$$

the relationship between the torsional moment (M_{tor}) and the rotation (θ).

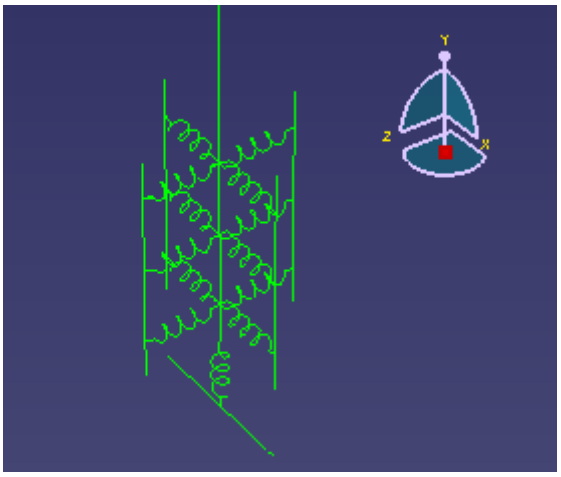

Figure 19: Soil model

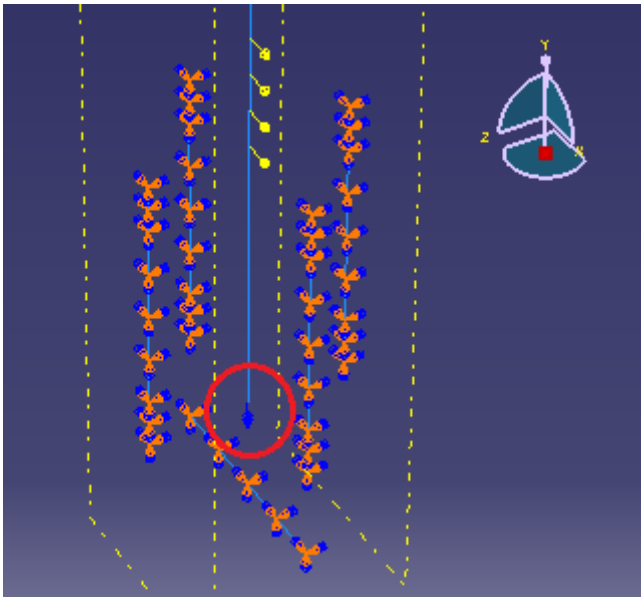

Figure 20: Rotational boundary condition (red marked)

3.3.3 Load cases

Three load cases have been considered in the analysis to cover the fatigue and ultimate limit state assessments, operational conditions (1), maximum operational conditions (2) and maximum wind (3).

All load cases have the same hub and nacelle weight, which is given by the selected turbine, 6.2M126 (previous RePower 6M) (Senvion, 2014) and according to the fictitious selected location, the water depth has been fixed in 40 m.

The wave, current and wind loads have been calculated as in (Lozano-Minguez, Kolios, & Brennan, 2011), assuming the same conditions; where the wave loads have been calculated by the third-order Stokes wave theory in combination with the Morison equation; the current loads have been calculated according to (Wilson, 2003), taking into account the current is generated on one part by the tide and on another part by the local wind; the wind loads have been calculated from the gust wind speed with a drag coefficient. It has been considered that the wave and current loads are the same in all cases.

Fx [N]	Fz [N]
550460.43	**524501.01**

Table 3: Wave loads

		Dp = 3 m	Dp = 4 m	Dp = 5 m	Dp = 6 m	Dp = 7 m	Dp = 8 m
y [m]	u(y)	F_y [N/m]	F_y [N/m]	F_y [N/m]	F_y [N/m]	F_y [N/m]	F_y [N/m]
-4	0.97	**1873.07**	**1873.07**	**1873.07**	**1873.07**	**1873.07**	**1873.07**
-4	0.97	**936.53**	**1248.71**	**1560.89**	**1873.07**	**2185.24**	**2497.42**
-12	0.90	**809.96**	**1079.94**	**1349.93**	**1619.92**	**1889.90**	**2159.89**
-20	0.82	**679.51**	**906.01**	**1132.51**	**1359.01**	**1585.51**	**1812.01**
-28	0.73	**537.81**	**717.08**	**896.35**	**1075.62**	**1254.89**	**1434.17**
-36	0.60	**354.69**	**472.93**	**591.16**	**709.39**	**827.62**	**945.85**

Table 4: Current loads by pile diameter (Dp) and depth (y)

3.3.3.1 Operational conditions

This load case is necessary to carry out the fatigue limit state assessment, as the fatigue is produced by the loading cycles generated under the operational conditions. Under these conditions the structure must withstand the

aerodynamic, wind, wave and current loads, apart from the hub and nacelle weights.

v [m/s]	F_x [N]	F_y [N]	F_z [N]	M_x [Nm]	M_y [Nm]	M_z [Nm]
10	**1.08 E+06**	**8.40 E+04**	**-3.48 E+06**	**5.28 E+06**	**-1.11 E+07**	**-3.7 E+06**

Table 5: Operational aerodynamic loads

Source: (Subroto, 2006)

which orientation can be founded in (Subroto, 2006). The wind loads have been calculated following the procedure mentioned above, with a gust wind speed of 10 m/s.

y [m]	Diameter [m]	Thickness [m]	u(z)	F_y [N/m]
2.5	6	0.05	8.705505633	**177.34**
9.865	6	0.025	9.986417279	**233.36**
19.595	5.76	0.02375	10.69583087	**256.99**
29.325	5.52	0.0225	11.13586102	**266.96**
39.055	5.28	0.02125	11.45955265	**270.42**
48.785	5.06	0.02	11.71732918	**270.94**
58.515	4.82	0.01875	11.93237026	**267.65**
68.245	4.58	0.0175	12.11733414	**262.27**
77.975	4.34	0.01625	12.27992002	**255.24**
87.705	4.1	0.015	12.42517274	**246.86**

Table 6: Wind operational loads

3.3.3.2 Maximum operational conditions

The ultimate limit state assessment has to be verified for the extreme conditions the structure must withstand. The maximum operational condition is that one in which the aerodynamic loads are maximum. The extreme aerodynamic loads are given by (Subroto, 2006) for our wind turbine:

v [m/s]	F_x [N]	F_y [N]	F_z [N]	M_x [Nm]	M_y [Nm]	M_z [Nm]
12	**1.15 E+06**	**8.20 E+04**	**-3.49 E+06**	**5.27 E+06**	**-1.30 E+07**	**-4.10 E+06**

Table 7: Extreme aerodynamic loads

Source: (Subroto, 2006)

which orientation can be founded in (Subroto, 2006). And for this case the wind gust is 12 m/s.

y [m]	Diameter [m]	Thickness [m]	u(z)	F_y [N/m]
2.5	6	0.05	10.44660676	**255.37**
9.865	6	0.025	11.98370074	**336.05**
19.595	5.76	0.02375	12.83499704	**370.07**
29.325	5.52	0.0225	13.36303322	**384.43**
39.055	5.28	0.02125	13.75146318	**389.40**
48.785	5.06	0.02	14.06079502	**390.15**
58.515	4.82	0.01875	14.31884431	**385.41**
68.245	4.58	0.0175	14.54080097	**377.67**
77.975	4.34	0.01625	14.73590403	**367.54**
87.705	4.1	0.015	14.91020729	**355.48**

Table 8: Wind loads

3.3.3.3 Maximum wind load

The second load case to verify the ultimate limit state is in which the wind load is maximum, where the maximum gust wind speed is 35 m/s in our case. When the wind speed becomes so fast, the aerodynamic loads are not present, as the turbine does not work under this condition (Senvion, 2014).

y [m]	Diameter [m]	Thickness [m]	u(z)	F_y [N/m]
2.5	6	0.05	30.46926972	**2172.40**
9.865	6	0.025	34.95246048	**2858.72**
19.595	5.76	0.02375	37.43540803	**3148.13**

29.325	5.52	0.0225	38.97551357	**3270.30**
39.055	5.28	0.02125	40.10843427	**3312.61**
48.785	5.06	0.02	41.01065213	**3319.01**
58.515	4.82	0.01875	41.7632959	**3278.70**
68.245	4.58	0.0175	42.41066948	**3212.78**
77.975	4.34	0.01625	42.97972008	**3126.67**
87.705	4.1	0.015	43.4881046	**3024.05**

Table 9: Maximum wind loads

3.3.4 Tower

Considering the characteristics of the selected wind turbine, the geometry for the tower has been modelled in nine linear pieces with the same length, rising 87.57 m, but variable diameter from 6 m to 4.1 m and also variable thickness due to fatigue assessment (see table 6).

4 CASE STUDY

From the soil properties map generated through RBF, three different pairs of soil properties have been selected, each from a different soil type, to compare their effect over the foundation design.

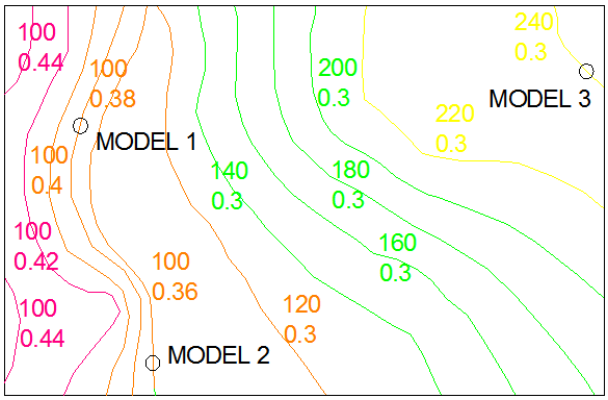

Figure 21: Selected soil data

	E [MPa]	v
MODEL 1	100	0.38
MODEL 2	100	0.36
MODEL 3	240	0.3

Table 10: Model soil properties

4.1 Comparative analysis

Depending on the stiffness of the soil, different resistance requirements will be required from the analysis in order to accommodate the environmental and operational loads, hence an iterative process should be employed towards optimizing the design of components in order to perform with adequate reliability (respecting the ALARP principals).

4.1.1 Comparative analysis Model 1

Following the process explained before, for the clay soil, the results from the analysis are given in tables 11-13:

				Tower-T.Piece		T.Piece-Pile	
D [m]	**Thickness [m]**	**L_{pile} [m]**	**V_{steel} [m^3]**	**σ_v^1 [Pa]**	**σ_v^1 [MPa]**	**σ_v^2 [Pa]**	**σ_v^2 [MPa]**
7	0.1	30	65.03096793	2.54E+07	**25.42**	1.24E+07	**12.39**
7	0.08	30	52.17557079	2.54E+07	**25.42**	1.24E+07	**12.39**
7	0.06	30	39.24477543	2.54E+07	**25.42**	1.24E+07	**12.39**
7	0.04	30	26.23858184	2.54E+07	**25.42**	1.24E+07	**12.39**
6	0.06	30	33.58990865	2.54E+07	**25.42**	1.24E+07	**12.39**
5	0.08	30	37.09592605	2.54E+07	**25.42**	1.24E+07	**12.39**
4	0.1	30	36.75663405	2.54E+07	**25.42**	1.24E+07	**12.39**
4	0.09	30	33.16579364	2.54E+07	**25.42**	1.24E+07	**12.39**

Table 11: Comparative analysis Case 1 - Model 1

D [m]	**Thickness [m]**	**L_{pile} [m]**	**V_{steel} [m^3]**	**Disp. Max [m]**	**σ_v [Pa] T-TP**	**σ_v [Pa] max**	**ɣ**
7	0.1	30	65.03096793	**1.01758**	2.74E+07	8.69E+07	**4.08**
7	0.08	30	52.17557079	**1.03785**	2.74E+07	8.69E+07	**4.08**
7	0.06	30	39.24477543	**1.07721**	2.74E+07	8.69E+07	**4.08**
7	0.04	30	26.23858184	**1.17423**	2.74E+07	8.69E+07	**4.08**
6	0.06	30	33.58990865	**1.0903**	2.74E+07	8.69E+07	**4.08**
5	0.08	30	37.09592605	**1.07033**	2.74E+07	8.69E+07	**4.08**
4	0.1	30	36.75663405	**1.09481**	2.74E+07	8.69E+07	**4.08**
4	0.09	30	33.16579364	**1.11389**	2.74E+07	8.69E+07	**4.08**

Table 12: Comparative analysis Case 2 - Model 1

D [m]	Thickness [m]	L_{pile} [m]	V_{steel} [m^3]	Disp. Max [m]	σ_v [Pa] T-TP	σ_v [Pa] max	ɣ
7	0.1	30	65.03096793	**2.61896**	2.61E+07	2.61E+07	**13.60**
7	0.08	30	52.17557079	**2.64128**	2.61E+07	2.61E+07	**13.60**
7	0.06	30	39.24477543	**2.67925**	2.61E+07	2.69E+07	**13.21**
7	0.04	30	26.23858184	**2.75792**	2.61E+07	4.01E+07	**8.85**
6	0.06	30	33.58990865	**2.74888**	2.61E+07	3.59E+07	**9.89**
5	0.08	30	37.09592605	**2.80132**	2.61E+07	3.83E+07	**9.26**
4	0.1	30	36.75663405	**2.95761**	2.61E+07	4.77E+07	**7.45**
4	0.09	30	33.16579364	**3.00498**	2.61E+07	5.27E+07	**6.74**

Table 13: Comparative analysis Case 3 – Model 1

These tables show, for the case 1, the stresses at tower-transition piece connection (σ_v^1) and transition piece-pile joint (σ_v^2); and for the cases 2 and 3, the maximum displacement of the top of the tower (Disp. Max), the maximum stress (σ_v max) regardless of its location, and the stress at the joint between the tower and the transition piece (σ_v T-TP), for each studied pile geometry. The global safety factor (ɣ) has been obtained from the maximum stress, in order to check the most unfavourable situation.

Case 1 is which studies the fatigue, while case 2 is which studies the maximum operational loads and case 3 studies the maximum wind condition, last both to check the ultimate limit state. Following the trial and error process it has been obtained different acceptable geometries for this soil, under the different load cases, meeting the requirements for both limit states.

According to the considered conditions, based on the pile length (L_{pile}) for this model (30 m), the maximum acceptable deflection at hub height in this case is 3.25 m, which is the 2% of the total length of the structure. And as it was calculated before, the minimum acceptable global safety factor to our structure is 1.55.

4.1.2 Comparative analysis Model 2

Following exactly the same process which was followed in the previous step, it was obtained for the dense sand:

				Tower-T.Piece		T.Piece-Pile	
D [m]	**Thickness [m]**	**L_{pile} [m]**	**V_{steel} [m^3]**	**σ_v^1 [Pa]**	**σ_v^1 [MPa]**	**σ_v^2 [Pa]**	**σ_v^2 [MPa]**
4	0.03	20	7.483273701	3.17E+07	**31.73**	3.58E+07	**35.75**
4	0.04	20	9.952565527	3.17E+07	**31.73**	3.08E+07	**30.77**
3	0.05	20	9.267698328	3.17E+07	**31.73**	3.30E+07	**32.95**
3	0.04	20	7.439291404	3.17E+07	**31.73**	4.10E+07	**40.98**

Table 14: Comparative analysis Case 1 - Model 2

D [m]	**Thickness [m]**	**L_{pile} [m]**	**V_{steel} [m^3]**	**Disp. Max [m]**	**σ_v [Pa] T-TP**	**σ_v [Pa] max**	**ɣ**
4	0.03	20	7.483273701	-	**-**	**-**	-
4	0.04	20	9.952565527	**0.643**	3.42E+07	8.69E+07	**4.08**
3	0.05	20	9.267698328	**0.692**	3.42E+07	8.69E+07	**4.08**
3	0.04	20	7.439291404	-	-	-	-

Table 15: Comparative analysis Case 2 - Model 2

D [m]	**Thickness [m]**	**L_{pile} [m]**	**V_{steel} [m^3]**	**Disp. Max [m]**	**σ_v [Pa] T-T.P.**	**σ_v [Pa] max**	**ɣ**
4	0.03	20	7.483273701	-	**-**	**-**	-
4	0.04	20	9.952565527	**1.242**	3.26E+07	1.16E+08	**3.07**
3	0.05	20	9.267698328	**2.097**	3.26E+07	1.63E+08	**2.18**
3	0.04	20	7.439291404	-	-	-	-

Table 16: Comparative analysis Case 3 – Model 2

As in this model the pile length is 20 m, the maximum acceptable deformation is 3.05 m, a bit lower than in the previous model, as the pile length is 10 m shorter.

For this soil type, as it is stronger, the required diameters are smaller than for the clay type, therefore the structure has been analyzed to the diameters which are necessary for the structure.

Observing table 14, we can see as it has been highlighted in red two of the results, this has been because the obtained stress at the connection between the transition piece and the pile (σ_v^2), exceed the maximum admissible (33.3 MPa) to meet the fatigue assessment; so keeping that geometry, the structure would fail by fatigue. The next simulation has increased the thickness for the first case (0.04 m) and in the second one means that we cannot reduce the thickness for that diameter (3 m).

Although the loads are almost the same as the ones from the previous soil type, as the soil is able to resist much more, it restricts more the displacements, so there is less deformation. But in this case, the geometry of the foundation is slimmer and also the movement is restricted, thus the stresses are larger than for the clay soil.

4.1.3 Comparative analysis Model 3

Finally, for the third soil conditions, very dense sand, it has been obtained the next comparative analysis:

				Tower-T.Piece		T.Piece-Pile	
D [m]	**Thickness [m]**	**L_{pile} [m]**	**V_{steel} [m^3]**	**σ_v^1 [Pa]**	**σ_v^1 [MPa]**	**σ_v^2 [Pa]**	**σ_v^2 [MPa]**
4	0.03	20	7.483273701	3.17E+07	**31.73**	3.58E+07	**35.75**
4	0.04	20	9.952565527	3.17E+07	**31.73**	3.08E+07	**30.77**
3	0.05	20	9.267698328	3.17E+07	**31.73**	3.30E+07	**32.95**
3	0.04	20	7.439291404	3.17E+07	**31.73**	4.10E+07	**40.98**

Table 17: Comparative analysis Case 1 - Model 3

D [m]	Thickness [m]	L_{pile} [m]	V_{steel} [m^3]	Disp. Max [m]	σ_v [Pa] T-TP	σ_v [Pa] max	ɣ
4	0.03	20	7.483273701	-	-	-	-
4	0.04	20	9.952565527	**0.369**	3.42E+07	8.69E+07	**10.39**
3	0.05	20	9.267698328	**0.535**	3.42E+07	8.69E+07	**10.39**
3	0.04	20	7.439291404	-	-	-	-

Table 18: Comparative analysis Case 2 - Model 3

D [m]	Thickness [m]	L_{pile} [m]	V_{steel} [m^3]	Disp. Max [m]	σ_v [Pa] T-TP	σ_v [Pa] max	ɣ
4	0.03	20	7.483273701	-	-	-	-
4	0.04	20	9.952565527	**1.1649**	3.26E+07	1.16E+08	**3.07**
3	0.05	20	9.267698328	**2.0413**	3.26E+07	1.63E+08	**2.18**
3	0.04	20	7.439291404	-	-	-	-

Table 19: Comparative analysis Case 3 - Model 3

where, exactly the same as in the previous model, the pile length (L_{pile}) is 20 m, so the maximum acceptable deformation is 3.05 m.

The considered geometries in this model have been the same as the ones considered in model 2 and as the loads are the same, it has been obtained that the deformation is smaller than for the dense sand conditions, as the soil is even stronger. We can see again as there are two pile geometries that would not resist the cyclic loading and would fail by fatigue.

Comparing the obtained results under the third load case (extreme wind), for the soils, dense sand and very dense sand, we can see as they are practically the same; that is why the geometry of the tower does not change between the models, then the wind loads do not change under the same load case. At the same time, the pile geometries considered for these both soils are the same; so the small difference obtained between the results is due to the different soil resistance.

4.1.4 Comparative analysis between soils

Having found different optimum geometries for every soil condition, a separate analysis has considered the behaviour of the same geometry for the complete structure, in the different soil condition scenarios. It has been selected a monopile foundation with 5 m of diameter, 30 m length and 0.08 m thickness, which results are shown in the next tables.

SOIL	Tower-T.Piece σ_v^1 [MPa]	T.Piece-Pile σ_v^2 [MPa]
CLAY	**25.42**	**12.39**
DENSE SAND	**25.42**	**12.39**
VERY DENSE SAND	**25.42**	**12.39**

Table 20: Analysis load case 1

SOIL	Disp. Max [m]	σ_v [MPa] Tower-T.Piece	ɣ
CLAY	**1.07**	27.4	**4.08**
DENSE SAND	**0.324**	27.4	**4.08**
VERY DENSE SAND	**0.189**	27.4	**4.08**

Table 21: Analysis load case 2

SOIL	Disp. Max [m]	σ_v [MPa] Tower-T.Piece	ɣ
CLAY	**2.801**	26.1	**9.26**
DENSE SAND	**0.435**	26.1	**9.26**
VERY DENSE SAND	**0.394**	26.1	**9.26**

Table 22: Analysis load case 3

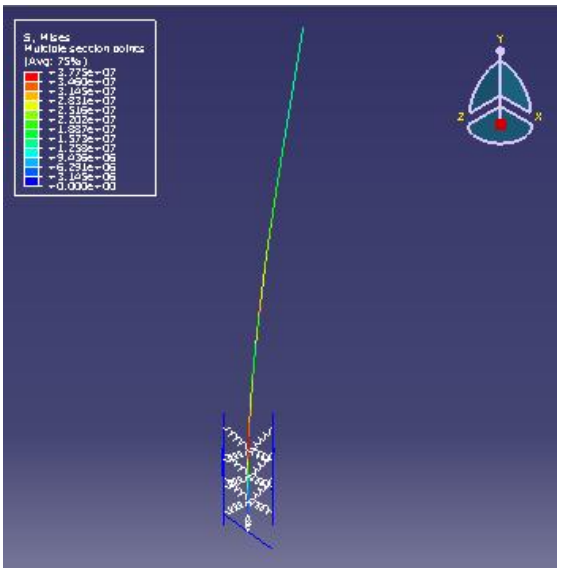

Figure 22: Von Mises stresses represented over the deform shape for load case 3

We can see as the maximum stress appears when the soil interaction affects the structure (see figure 22), which means when the soil restricts the movement; but this stress is not realistic, because the springs represent 10 m of soil column, that is why this point cannot be taken as comparative. The comparison stresses have been selected at the bottom of the tower level, on its joint with the transition piece, as well as at the connection between the transition piece and the pile; because these points represent a discontinuity or weak point for the structure.

In the last comparative analysis, for the same structure geometry considering different soil scenarios, we can see as under the same load case the stresses are the same at both considered points, tower-transition piece and transition piece-pile, although the deformation at the top of the tower is not the same. This can be explained by the redistribution of stresses, which means the stress excess at the top of the tower is supported by the tower, redistributed along its length, and then the stress at tower-transition piece level is the same.

Observing tables 21 and 22, we can see as the top tower deformation (Disp. Max) is different for different soil conditions with the same geometry under the same load case, which means the resistance is different on each selected soil; as the soil is stronger, less deformation occurs.

Comparing the obtained results from both sandy soils (models 2 and 3), as the considered geometries are the same for both of them, we can see as the stresses are the same for the same load case, although there is a small difference between their deflections at the top of the tower, where the stronger soil presents less deformation. This is due to the previous given explanations, stress redistribution and soil resistance.

In the comparative analysis by model, we could see as the stress is always the same for different geometries under the same soil conditions and the same load case at tower-transition piece level; this is because the tower is longer enough to redistribute the stresses along its length for all cases (see tables 11-19 and figure 23). On the other hand, under the same soil conditions and load case, the stresses sometimes are not the same for different pile geometries at transition piece-pile level (tables 14 and 17 and figure 24); this just can be explained by the slimness of the piles, as it does not happen for the clay soil, where the pile geometries are less slim. When the pile geometry is slimmer, the structure is more expose to the deformation and then to suffer higher stresses.

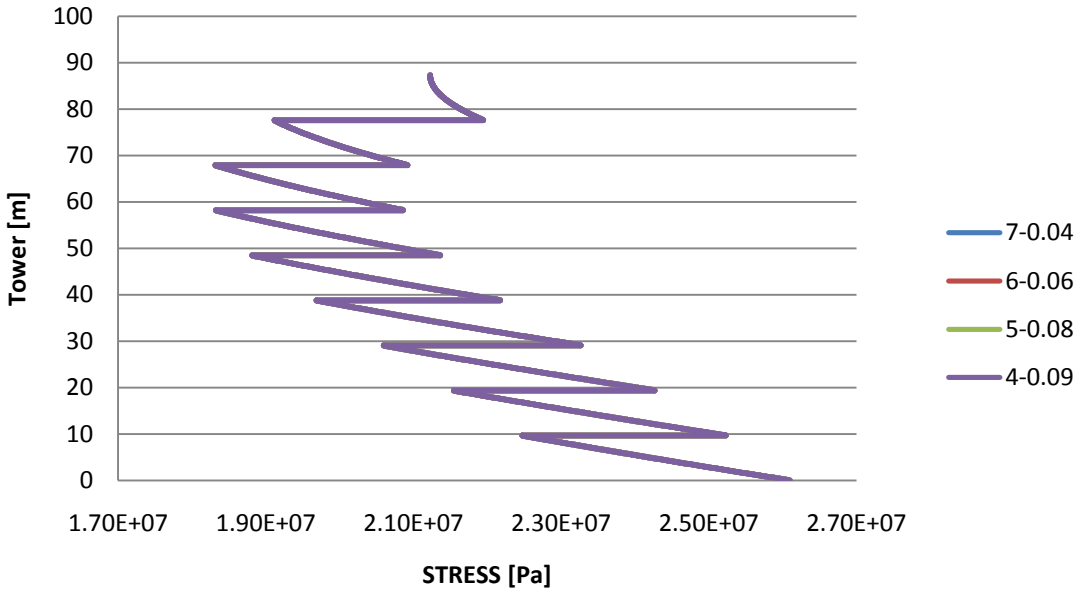

Figure 23: Stresses along tower for different pile geometries - Clay - Case 1

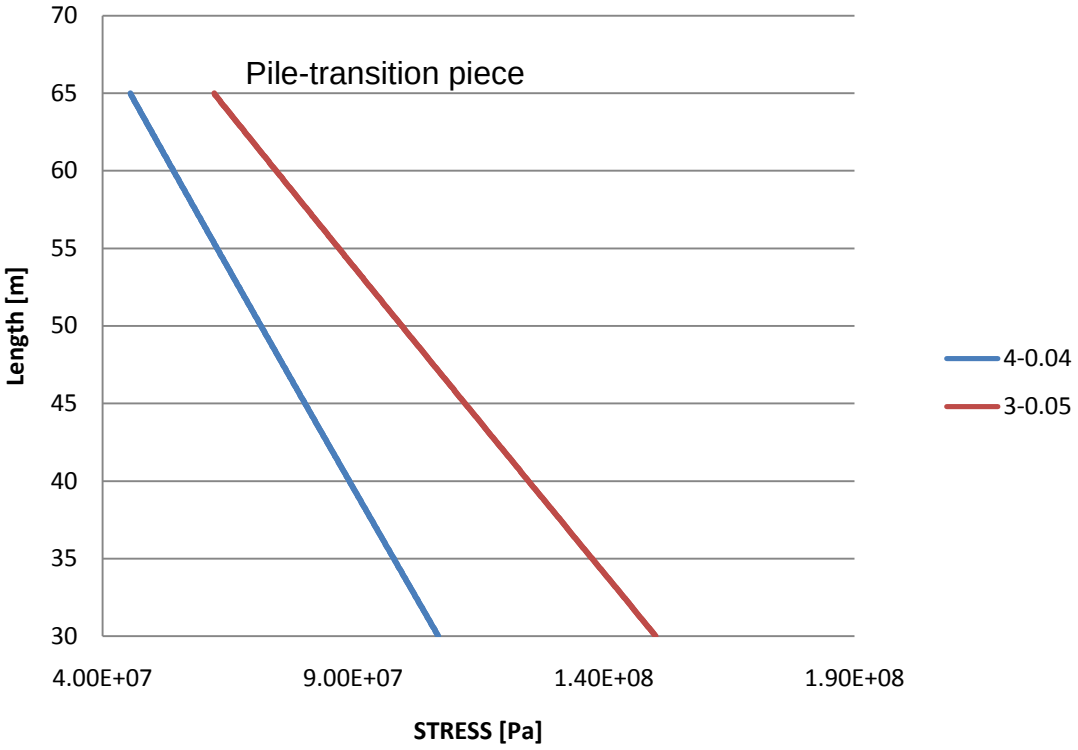

Figure 24: Stresses along pile (water) for different pile geometries - Very dense sand - Case 1

The global safety factors (γ) have been calculated with the maximum stress for each model. That maximum stress has been found sometimes at the top of the tower, due to the aerodynamic loads, or at the first spring level (soil); as it is not always located at the same point, it was not possible to take it as a comparative for all cases. But nevertheless, it has been used to calculate the safety factor in order to consider the most unfavourable situation. Although it can be overestimated (soil level), if it remains on the safety side, the structure meets the ultimate limit state stress requirement.

Also from the last analysis it can be seen as the design of these foundations is managed by the fatigue limit state, as the structures are able to withstand higher loads, but these must be punctual, otherwise the structure life would be shorter due to the fatigue.

Based on this comparative analysis it must be taken into account other aspects to select the optimum geometry for each soil type, as all those geometries meet

the design conditions. Aspects as material availability, fabrication process, storage, welding, fatigue test or corrosion have been taking into account to select the appropriate geometry for each model.

MODEL 1: the diameter-thickness combination which better fits the cost criteria, based on material availability, steel volume, fabrication, transport and assembly, is pile diameter 5 m and 8 cm of thickness, with pile length 30 m.

MODEL 2 and 3: as it is better to use as less different geometries as possible, and both of this models can use the same geometry, it will be used the same foundation for them. In this case, in order to reduce the slimness of the foundation, although it would be taken deepest account in the corrosion, the selected geometry has 20 m length for the piles, 4 m diameter and 4 cm of thickness.

4.2 Wind farm layout

In order to optimize the use of the wind, offshore wind farms are laid out in a specific configuration. The layout depends on the main wind direction to avoid turbulence from other wind turbines, where the minimum distance in main wind direction is 5-8 times rotor diameter (E.ON, 2012) and 3-5 times in the perpendicular direction.

As the used wind turbine is 6.2M126, the rotor diameter is 126 m. Following this thumb rule and assuming the main wind direction is east, the layout in this wind farm would be:

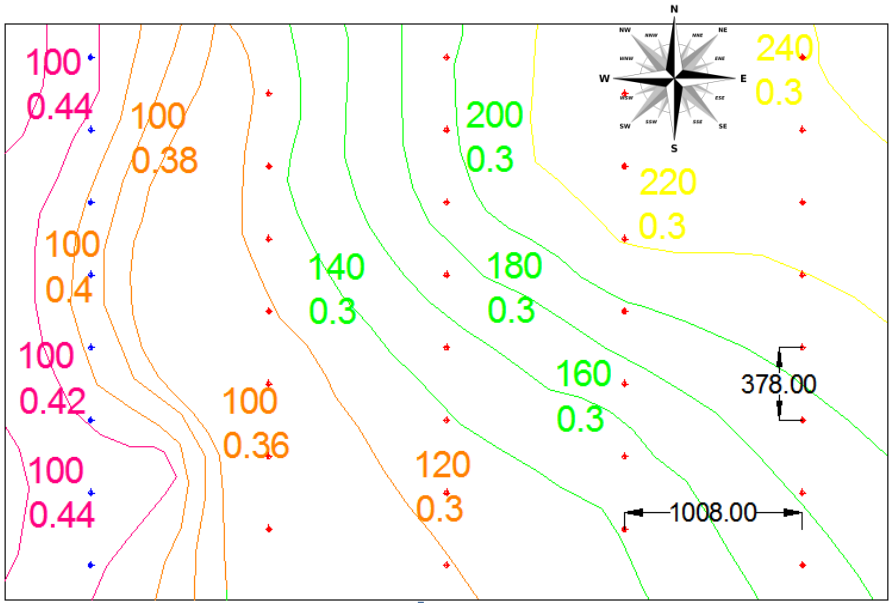

Figure 25: Wind farm layout

Where there are 38 wind turbines and it can be seen in red, the wind turbines with the geometry foundation corresponding to model 2 and 3, and in blue the wind turbines corresponding to model 1. These two different geometries show as the foundation cost for a wind turbine can increase even four times due to the soil conditions requirements.

5 CONCLUSIONS

5.1 Discussion

In general, although we cannot say one method is better than another one because it depends on each case, it could be said RBF will always be faster and more exact as far as the value of the variable at data points meets the data value and it has not to estimate the values at data points.

Logically we understand the accuracy of a method should be higher with a bigger amount of data points, which happens with RBF as it can be seen in figures 6 and 7. But observing the analysis results from Kriging, we can see as the accuracy in the prediction for Young's modulus is higher for 15 data points than for 20. And it happens exactly the same from Poisson's ratio between 7 and 15 data samples. This shows a weakness of the method, because we could not ensure higher accuracy by taking a bigger amount of data.

5.2 Assumptions and limitations of the methodology

This study has presented a methodology for the soil characterization of the offshore wind farms, in order to reduce the lack of knowledge about its geotechnical conditions. Considering the unavailability of real data to carry out the research, this offers in detail the process to follow, having considered fictitious data which could be real.

The calculated samples ratio is used to compare the required data points for the method and the amount of installed wind turbines in order to see if the site investigation cost could be reduced; but it cannot be taken as general rule, as it depends on the wind farm size and specially, on the variability of the variable values along the area.

The variables Young's modulus and Poisson's ratio have been considered constant by depth, which assumption is not real. Taking into account that they can change by depth, also other interpolation techniques could have been used considering secondary information.

The estimated soil properties to characterize the wind farm are based on Winkler soil modelling method, which is not the most accurate. If the FEA would use i.e. a 3D soil model, other soil properties such specific gravity should be considered.

Due to the lack of information in the standards, the maximum allowable deflection has been considered the 2% of the total length of the structure. This limit value should be calculated studying the maximum deflection under the wind turbines operate, as well as the maximum registered deformation before bending failure in past accidents, to check which situation corresponds with the ultimate state of failure.

The foundation design analysis should be completed to ensure the structure support against other phenomenons, i.e. buckling, as this was just a first basis analysis.

5.3 Achievements

This paper has presented a methodology for predicting the soil properties over the total affected area by a wind farm, in order to reduce the installation cost of this machines and then to reduce the LCOE. From a limited amount of data (20 sample points) it has been possible to predict the soil properties reaching an accuracy of 90% or higher. The data ratio of 1.33 samples/km^2 has been probed as smaller than the amount of wind turbines that could be installed on the entire area; considering that its ratio is 2.53 turbines/km^2, this leads to suppose a 50% reduction in site investigation cost, taking into account that this cost depends only on the number of needed samples.

Also the fact to know the soil properties over the total area makes a reduction in the total cost, as it will not appear unexpected costs due to the lack of soil characterization.

Comparing the foundation geometries necessary for each soil type and supposing that the foundation cost depends only on the steel volume, we would have in this wind farm 8 wind turbines (model 1) almost 4 times more expensive than the rest of them. Taking benefit on the soil characterization and making

use of the dispersion alternative, it is recommended changing the location of those 8 wind turbines to other locations either inside the same area or outside, depending on the benefit for the grid, as it is worth to reduce the foundation cost; regardless the increasing cabling cost.

5.4 Future work

The geotechnical conditions of the soil can fluctuate greatly across the wind farm. This is an issue since geotechnical modelling is the base of the structural design of an offshore wind farm. One way to deal with it is considering the soil properties as random variables and predict them there where they are unknown by using any of the available interpolation techniques, processing the samples.

To take greater benefit from this soil characterization, it could be calculated the failure probability of the structures at every single point of the wind farm, in order to base the wind turbine locations on its failure probability due to the soil conditions.

The soil properties interpolation gives us the uncertainty value of its prediction, with which by running a Monte Carlo based reliability simulation, can be obtained the probability of failure for each soil condition, with the suitability of a support structure.

REFERENCES

(EWEA), E. W. (2014). *EWEA Annual Report 2013.*

4COffshore. (2014). *4C Offshore*. Retrieved June 2014, from Global offshore wind farms database: http://www.4coffshore.com/windfarms/windfarms.aspx?windfarmid=UK09

Abdel-Rahman, K., & Achmus, M. (2005). *Finite element modelling of horizontally loaded monopile foundations for offshore wind energy converters in Germany.* Hannover: Institute of soil mechanics, foundation engineering and waterpower engineering.

Aysen, A. (2005). Soil mechanics: basic concepts and engineering applications. *London: Taylor & Francis* .

Bayona, V., Moscoso, M., & Kindelan, M. (2011). Optimal constant shape parameter for multiquadric based RBF-FD method. *Journal of Computational Physics 230* , 7384-7399.

BGS. (2014). *MAREMAP*. Retrieved August 8, 2014, from Marine Environmental Mapping Programme: http://www.maremap.ac.uk/index.html

Bishop, T., & Lark, R. (2007). A landscape-scale experiment on the changes in available potassium over a winter wheat cropping season. *Geoderma* , 384-396.

Bowles, J. (1996). *Foundation analysis and design.* New York: McGraw-Hill.

British Standard. (2006). Eurocode 3: Design of steel structures. *BS EN 1993-1-1:2005* .

BSH. (2008). Standard: Ground Investigations for Offshore Wind Farms.

Buren, E. V., & Muskulus, M. (2012). Improving pile foundation models for use in bottom-fixed offshore wind turbine applications. *Energy Procedia* , 363-370.

Burgess, T., & Webster, R. (1980). Optimal interpolation and isarithmic mapping of soil properties. I. The semivariogram and punctual kriging. *Journal of Soil Science* , 315-331.

Burrough, P., & Mcdonnell, R. (1998). Principles of geographic information systems. Oxford University Press.

Cameron, T., Crosby, A., Balson, P., Jeffery, D., Lott, G., Bulat, J., et al. (1992). *United Kingdom Offshore Regional Report: The Geology of the Southern North Sea.* London: HMSO.

Carr, J., Fright, W., & Beatson, R. (2002). Surface interpolation with radial basis functions for medical imaging. *IEEE Transactions on Medical Imaging* , 96-107.

Carswell, W., Arwade, S. R., DeGroot, D. J., & Lackner, M. A. (2014). Soil–structure reliability of offshore wind turbine monopile foundations. *Wind energy* .

Chen, W.-F., & Duan, L. (1999). *Bridge engineering handbook.* USA: CRC Press.

Chica-Olmo, M., Luque-Espinar, J. A., Rodriguez-Galiano, V., Pardo-Igúzquiza, E., & Chica-Rivas, L. (2014). Categorical indicator kriging for assesing the risk of groundwater nitrate pollution: the case of Vega de Granada aquifer (SE Spain). *Science of The Total Environment* , 229-239.

Collins, F., & Bolstad, P. (1996). A comparison of spatial interpolation techniques in temperature estimation. *Third International Conference/Workshop on Integrating GIS and Environmental Modeling.* Santa Barbara: Proceedings.

Dai, F., Zhou, Q., Lv, Z., Wang, X., & Liu, G. (2014). Spatial prediction of soil organic matter content integrating artificial neural network and ordinary kriging in Tibetan Plateau. *Ecological Indicators* , 184-194.

Department of Energy & Climate Change. (2011). *UK renewable energy roadmap.*

Dicorato, M., Forte, G., Pisani, M., & Trovato, M. (2011). Guidelines for assessment of investment cost for offshore wind generation. *Renewable energy* , 2043-2051.

DNV. (2010). *DNV-OS-J101: Design of Offshore Wind Turbine Structures.*

E.ON. (2012). *E.ON offshore wind energy factbook.* E.ON Climate & Renewables.

Gatliff, R., Richards, P., Smith, K., Graham, C., McCormac, M., Smith, N., et al. (1994). *United Kingdom Offshore Regional Report: The Geology of the Southern North Sea.* London: HMSO.

Gerolymos, N., & Gazetas, G. (2006). Winkler model for lateral response of rigid caisson foundations in linear soil. *Soil Dynamics and Earthquake Engineering* , 347-361.

Gong, G., Mattevada, S., & O'Bryant, S. E. (2014). Comparison of the accuracy of kriging and IDW interpolations in estimating groundwater arsenic concentrations in Texas. *Environmental Research* , 59-69.

Goovaerts, P. (2001). Geostatistical modelling of uncertainty in soil science. *Geoderma* , 3-26.

Hamilton, E. (1971). Elastic properties of marine sediments. *Journal of Geophysical Research 76* , 579 - 604.

Hamilton, E. L. (1979). Vp/Vs and Poisson's ratio in marine sediments and rocks. *J. Acoust. Soc. Am., Vol.66* , 1093 - 1101.

Hare, S. O., & Harwood, N. (2013). Soil structure interaction starts with engineers. *NZSEE Conference* .

Hartkamp, A., De Beurs, K., Stein, A., & White, J. (1999). *Interpolation techniques for climate variables.* Mexico: CIMMYT.

Heidari, M., Naggar, H. E., Jahanandish, M., & Ghahramani, A. (2014). Generalized cyclic p–y curve modeling for analysis of laterally loaded piles. *Soil Dynamics and Earthquake Engineering* , 138-149.

Henderson, A. R., & Zaaijer, M. B. (2008). Hydrodynamic loading on offshore wind turbine support structures. *Engineering integrity* , 24-31.

Henderson, A., & Camp, T. (2001). Hydrodynamic loading of offshore wind turbines. *European wind energy conference.* Copenhagen.

Higgins, P., & Foley, A. (2014). The evolution of offshore wind power in the United Kingdom. *Renewable and Sustainable Energy Reviews* , 599-612.

International Energy Agency, (. (2013). *Technology Roadmap, wind energy.* www.iea.org.

Isaaks, e., & Srivastava, R. (1989). *Applied geostatistics.* New York: Oxford University Press.

Jeong, S., Murayama, M., & Yamamoto, K. (2004). *Efficient optimization design method using kriging model.* Japan: Institute of Space Technology and Aeronautics.

Journel, A., & Huijbregts, C. (1978). *Mining Geostatistics.* London: Academic Press.

Karydas, C., Gitas, I. Z., Koutsogiannaki, E., Lydakis-Simantiris, N., & Silleos, G. N. (2009). Evaluation of spatial interpolation techniques for mapping agricultural topsoil properties in Crete. *EARSeL eProceedings 8* , 26-39.

Kazemi Poshtmasari, H., Tahmasebi Sarvestani, Z., Kamkar, B., Shataei, S., & Sadeghi, S. (2012). Comparison of interpolation methods for estimating pH and EC in agricultural fields of Golestan province (north Iran). *International Journal of Agriculture and Crop Sciences* , 157-167.

Kezdi, A. (1974). *Handbook of soil mechanics.* Amsterdam: Elsevier.

Kikuchi, Y., & Kimura, M. (2007). *Advances in deep foundations.* London: Taylor & Francis Group.

Koehler, J., & Owen, A. (1996). Handbook of statistics. In J. Koehler, & A. Owen, *Handbook of statistics* (pp. 261-308). Amsterdam: Elsevier.

Krivoruchko, K., & Gotay, C. (2003). Using spatial statistics in GIS. *International Congress on Modelling and Simulation* (págs. 713-736). D. A. Post.

Kulhawy, F. H., & Phoon, K.-K. (1996). Engineering judgement in the evolution from deterministic to reliability-based foundation design. *Uncertainty in the geologic environment* .

Lark, R., Dove, D., Green, S., Richardson, A., Stewart, H., & Stevenson, A. (2012). Spatial prediction of seabed sediment texture classes by cokriging from a legacy database of point observations. *Sedimentary geology* , 35-49.

Lefebvre, S., & Collu, M. (2012). Preliminary design of a floating support structure for a 5 MW offshore wind turbine. *Ocean Engineering* , 15-26.

Li, J., & D. Heap, A. (2008). *A review of spatial interpolation methods for environmental scientist.* Canberra: Geoscience Australia.

Li, J., Heap, A. D., Potter, A., Huang, Z., & Daniell, J. J. (2011). Can we improve the spatial predictions of seabed sediments? A case study of spatial interpolation of mud content across the southwest Australian margin. *Continental Shelf Research* , 1365-1376.

Lozano-Minguez, E., Kolios, A., & Brennan, F. (2011). Multi-criteria assessment of offshore wind turbine support structures. *Renewable Energy, Vol. 36* , 2831-2837.

Mabit, L., & Bernard, C. (2007). Assessment of spatial distribution of fallout radionuclides through geostatistics concept. *Journal of Environmental Radioactivity* , 206-219.

Mader, C. L. (2005). *Numerical modeling of water waves.* Florida: CRC Press.

Matheron, G. (1963). Principles of geostatistics. *Economic Geology* , 1246-1266.

Mohandes, M., Balghonaim, A., Kassas, M., Rehman, S., & Halawani, T. (2000). Use of radial basis functions for estimating monthly mean daily solar radiation. *Solar Energy* , 161-168.

Negro, V., Gutierrez, J.-S. L., Esteban, M. D., & Matutano, C. (2014). Uncertainties in the design of support structures and foundations for offshore wind turbines. *Renewable energy* , 125-132.

Prat, M., Bisch, E., Millard, A., Mestat, P., & Cabot, G. (1995). *La modelisation des ouvrages.* Paris: Hermes.

Randolph, M., Cassidy, M., Gourvenec, S., & Erbrich, C. (2005). Challenges of offshore geotechnical engineering. *XVI ICSMGE.* Osaka: Millpress Vol. 1.

RenewableUK. (2014). *RenewableUK*. Retrieved 7 23, 2014, from RenewableUK: http://www.renewableuk.com/en/renewable-energy/wind-energy/offshore-wind/

RESCO. (2014). *Renewable Energy Supply Chain Opportunities.* Retrieved August 8, 2014, from http://www.resco.org.uk/wind-and-marine-power/

Rouhani, S., Srivastava, R., Desbarats, A., Cromer, M., & Johnson, A. (1996). *Geostatistics for environmental and geotechnical applications.* ASTM International.

Sarra, S. A., & Kansa, E. J. (2009). *Multiquadric radial basis function approximation methods for the numerical solution of partial differential equations.*

Scharff, R., & Siems, M. (2013). Monopile foundations for offshore wind turbines – solutions for greater water depths. *Steel Construction* , 47-53.

Selvadurai, A. (1979). *Elastic analysis of soil-foundation interaction.* Amsterdam: Elsevier Scientific Publishing Company.

Senvion. (2014). *SENVION.* Retrieved May 2014, from http://www.senvion.com/fileadmin/user_upload/02_WindPowerSolutions/DataSheets/Senvion_6.2M126_Datasheet_EN.pdf

Subroto, H. (2006). *Bottom Founded Steel Support Structure for Offshore Wind Turbines in deeper waters of the North Sea.* Delft: Faculty of Aerospace Engineering.

Terzaghi, K. (1955). Evaluation of coefficients of subgrade reaction. *s.l.: Geotechnique* , 297-326.

The Crown Estate. (2012). *Offshore wind cost reduction. Pathways study.*

Van Assen, V. (2012). *The benefits of geographical dispersion of offshore wind turbines.* University of Groningen: Center for energy and environmental studies.

Verfaillie, E., Lancker, V. V., & Meirvenne, M. V. (2006). Multivariate geostatistics for the predictive modelling of the surficial sand distribution in shelf seas. *Continental shelf research* , 2454-2468.

Warrick, A. (1998). Spatial variability in environmental soil physics. *Academic Press, USA* , 655-675.

Webster. (1985). Quantitative spatial analysis of soil in the field. *Soil Sci* , 1-70.

Webster, R., & Oliver, M. (2001). *Geostatistics for Environmental Scientists.* Chichester: John Wiley & Sons, Ltd.

Wheeler, J. (1969). Method for calculating forces produced by irregular waves. *Offshore technology conference.* Dallas.

Wilson, J. F. (2003). *Dynamics of offshore structures.* New Jersey: John Wiley & Sons.

Winkler, E. (1867). Die Lehre von Elastizitat und Festigkeit. *Publisher* .

Yang, C.-S., Kao, S.-P., Lee, F.-B., & Hung, P.-S. (2012). *Twelve different interpolation methods: a case study of surfer 8.0.* National Chung Hsing University, Feng Chia University, Taichung.

Yin, J.-c., Zoua, Z.-j., & Xu, F. (2013, January). Sequential learning radial basis function network for real-time tidal level predictions. *Ocean Engineering* , 49-55.

Zandi, S., Ghobakhlou, A., & Sallis, P. (2012). A comparison of spatial interpolation methods for mapping soil pH by depths. *ANNA World 2011.* Chennai, India.

Zhong, R., & Huang, M. (2013). Winkler model for dynamic response of composite caisson-piles foundations: Lateral response. *Soil Dynamics and Earthquake Engineering* , 182-194.

Zhou, F., Guo, H.-C., Ho, Y.-S., & Wu, C.-Z. (2007). Scientometric analysis of geostatistics using multivariate methods. *Scientometrics* , 265-279.

Zimmermann, B., Zehe, E., Hartmann, N., & Elsenbeer, H. (2008). Analyzing spatial data: an assessment of assumptions, new methods, and uncertainty using soil hydraulic data. *Water Resources Research* , W10418.